ABSTRACT

ANIGULU MOHAN, DEEPAK KUMAR. Design of fully integrated wireless CMOS MEMS device for intraocular pressure measurement. (Under the direction of Dr. Paul D. Franzon and Dr. M.K.Ramasubramanian.)

The thesis research presented here explores the design and fabrication of wireless Integrated CMOS MEMS device for continuous intraocular pressure measurement. A complete study of the existing solutions for sensing intraocular pressure is made and the problems involved in them are identified in the report. A simple, low power, less invasive solution for the application is then proposed. Electromagnetic modeling of the inductive link is done and optimum dimensions for the antenna are finally suggested. Complete design of all the components of the system such as control circuit, power conversion and conditioning circuits, reference circuits necessary for reliable functioning of the device is presented. Integration of MEMS sensor along with the analog circuitry and antenna is detailed. Techniques for packaging the device in order to meet the standards for safe operation are then presented. The report has dedicated chapters on review of the existing sensors, Inductive link design, CMOS control and Power conditioning circuit, Sensor Integration and Packaging. The principles, methods, systems and circuits described in this thesis are applicable to other implantable wireless systems which have stringent requirements on power and space.

Design of fully integrated wireless CMOS MEMS device for intraocular pressure measurement

by
Anigulu Mohan Deepak Kumar

A thesis submitted to the Graduate Faculty of
North Carolina State University
in partial fulfillment of the
requirements for the degree of
Master of Science

ELECTRICAL ENGINEERING

Raleigh

2006

APPROVED BY:

Dr Paul D. Franzon	**Dr. M.K. Ramasubramanian**
(Chair of Advisory Committee)	(Co-Chair of Advisory Committee)

Dr. Kevin Gard
(Committee member)

Dedicated to my parents and teachers without whose support and guidance this thesis would not be possible. I express my gratitude to the Almighty who is the empowering energy of my life.

BIOGRAPHY

Anigulu Mohan Deepak Kumar is from an agricultural family based on Komakkambedu, a village near the city of Chennai, India. He received his Bachelor of Engineering in Electronics and Communications from University of Madras, India in May 2004. He focused his study in the area of Nanoelectronics and Microelectro-mechanical systems during his graduate study at North Carolina State University. He completed his Master of Science degree in May 2006. He has two publications in International conferences.

ACKNOWLEDGEMENTS

I would like to express my sincere appreciation to my advisors, Dr. Paul D. Franzon, Professor of Electrical and Computer Engineering and Dr. M.K. Ramasubramanian, Associate Professor of Mechanical and Aerospace engineering for their constant guidance. I convey my special thanks to my committee member Dr. Kevin Gard, William J. Pratt Assistant Professor of Electrical and Computer Engineering for his valuable suggestions during the research and Thesis report preparation .I express my thanks to Dr. Maysam Ghovanloo, Assistant Professor of Electrical and Computer Engineering for his help in getting the analog circuitry fabricated. I express my sincere thanks to Dr. Asrani who initiated this research. His mapping of the eye space and identification of the right spot for the implant has been the highlight of this research. I also thank Mr. Benjamin, Asia pacific sales director of Coventorware for providing me with the MEMS tools for evaluation. I thank Mr. Kalyan C. Katuri, PhD student of Dr M.K. Ramasubramanian for his help in CAD drawings. I express my gratitude to Dr. M.K. Ramasubramanian for his generous support during my thesis research. I thank Ms. Erica Braman for her help in editing this thesis report.

TABLE OF CONTENTS

Page

LIST OF TABLES

Page

LIST OF FIGURES

Page

LIST OF FIGURES (continued)

Page

LIST OF FIGURES (continued)

Page

CHAPTER 1

INTRODUCTION

Implantable microelectronics has revolutionized present day Health care especially in the area of Prosthesis, Diagnosis and Treatment. Ever since the pace maker, a large number of other biomedical implants have been proposed and designed for various medical problems and improving health care [1]. Most of these implants require the ability to transcutaneously accept commands from an external host system (e.g. computer, hand-held device) and/or to transmit physiological data outwards, as measured from inside the body [2]. The transfer of information is often achieved through a wireless interface established between transmission/reception antennas of the involved parts. Acquisition of physiological data in the implants is usually achieved through appropriate sensors while intervention to the human body if necessitated is achieved through actuators. The rapid advancement in this area has been fuelled by the exponential growth in microelectronics and micromachining capabilities in the past two decades. The thesis research is one such attempt which utilizes a CMOS-Integrated system for a biomedical application i.e. continuous measurement of intraocular pressure for detection and treatment of Glaucoma. .

1.1 Motivation for the Research

Glaucoma is a group of eye diseases, characterized by elevated intraocular pressure (IOP), which damages the optic nerve and leads to visual field loss, eventually leading to blindness if not treated. An estimated 67 million people suffer from glaucoma worldwide, including over 3 million Americans age 40 years and older [3]. Approximately 120,000 are blind from glaucoma; accounting for 9% to 12% of all cases of blindness in the U.S. Glaucoma is the

second leading cause of blindness in the U.S. and the first leading cause of irreversible blindness. Elevated intraocular pressure (IOP) is one of the most important risk factors of glaucoma, and it is the only treatable parameter for the disease at the present time. Current treatment is directed towards reducing the intraocular pressure (IOP) which has been shown to decrease disease progression. Early symptoms are detectable only by a physician. It is too late when the patient himself is able to feel a loss of vision. The condition is painless and cannot be detected without a pressure measurement, direct or indirect. Therefore, it is imperative to have an accurate measurement of the IOP in the case of glaucoma patients. Further, it is important to continuously monitor and control the IOP through implantable devices. Sensing the IOP continuously is, by itself a significant step in the detection and treatment of glaucoma. In the treatment phase, knowing that the pharmacologic treatment is working properly and the pressure never fluctuates or exceeds limits, will prevent disease complications and improve the efficiency of Glaucoma Treatment.

1.2 Organization of the thesis

The thesis is organized into 6 chapters, each explaining in detail a subsystem of the device.

The second chapter provides a detailed overview of the application, review of the existing solutions for the problem and identifies the challenges for the design. The third chapter explains the inductive link design which arrives at the optimum dimensions for the antenna. It uses circuit model for the inductive link and for determining the link parameters it makes use of an electromagnetic model. The design has been tested with electromagnetic field solving tools such as Fast Henry, Coventor MEMHenry and EM3DS.The fourth chapter explains in detail about the CMOS circuitry involved in the system. It is divided into two

sections. One is the design of the control circuitry and the other is the design of the power conversion and conditioning. The results of the simulations using cadence tool kit and the layout of this subsystem are presented. The circuits have been verified for all the process corners and few novel layout techniques have been implemented for reference circuits. The fifth chapter is dedicated to the post CMOS surface micromachining of the pressure sensor, antenna and their integration with the CMOS circuitry. This chapter also details the safe levels of operation of the device and the packaging used for the device. The sixth chapter provides the future direction for research and concludes by comparing the given design with those of other peer groups.

CHAPTER 2

REVIEW OF INTRAOCULAR PRESSURE SENSORS

The chapter gives a more detailed description about the source of intraocular pressure, its measurement, existing techniques used for the measurement, problems involved in these measurements and summary of the most important challenges in its design.

2.1 Intraocular pressure

A certain level of pressure is needed within the eye for it to keep its shape. This pressure is maintained by the flow of a fluid (aqueous humor) within the eye. The ocular fluid is formed by ciliary body as shown in Figure 1. It drains out of the eye at the angle and percolates through the trabecular meshwork (Appendix B) and flows into the canal of Schlem (Appendix B).

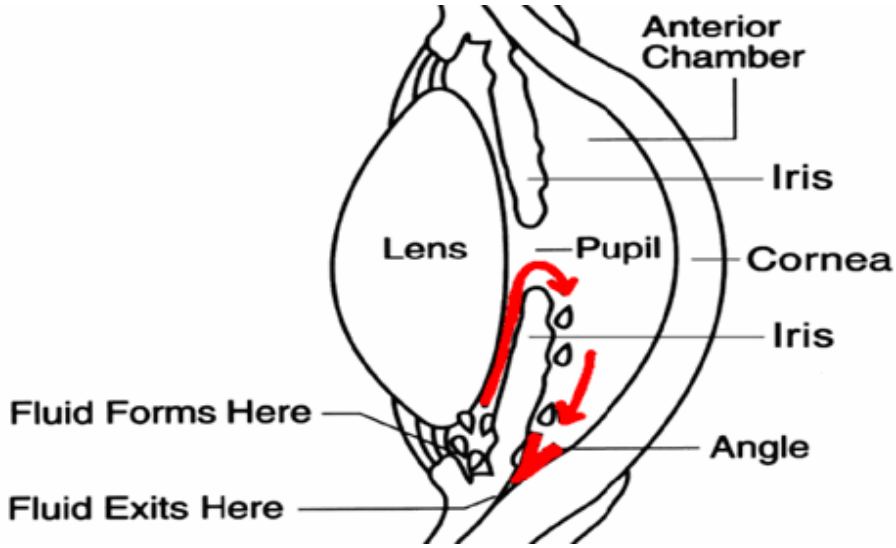

Figure 1. Formation and drainage of ocular fluid.

Ref: http://www.kellyeyecenter.com/images/glaucoma_crosssection.jpg

The cause of the elevated pressure is either clogging of fluid drainage system or over production of the aqueous fluid by the ciliary body. The clogging might be due to several reasons such as abnormal development of vessels obstructing trabecular meshwork. The resistance to flow presented by these tissues together with the aqueous humor production rate determine the final Intra Ocular Pressure (IOP). Increase in intraocular pressure or large fluctuations in pressure (discovered recently) damages the optic nerve (Figure 2) and leads to glaucoma. Glaucoma is the leading cause for irreversible blindness.

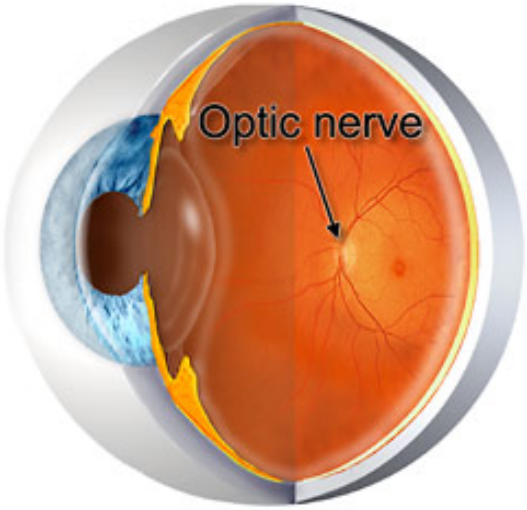

Figure 2. Location of optic nerve.

Ref:http://eyeMDlink.com

2.2 Review of existing solutions

The following section gives a brief overview of the existing solutions for measuring intraocular pressure.

2.2.1 Goldmann Applanation Tonometry

Goldmann Applanation Tonometer (GAT) which was introduced in 1950's has been the 'gold standard' for measuring IOP. Applanation tonometry uses a special probe to flatten part of the cornea to measure eye pressure with a slit lamp. Because the probe makes contact with the cornea, a topical eye anesthetic is introduced onto the surface of the eye in the form of one or a few eye drops. Yellow Fluorescein is also used to aid the examiner in determining the IOP. However, this instrument can only be used in a doctor's office, where a "snapshot" of the IOP is taken and is not portable.

2.2.1 Portable Hand-held tonometers

Over the years, various portable tonometers have been developed, and these include the Perkins [4], Tono-Pen [5], Zeimer's self-tonometer [6], Ocuton-S [7], and ProTon [8]. These instruments are costly and require a skilled operator.

2.2.3 Drawbacks of tonometers

As the pressure used to flatten cornea is used as an indicator of intraocular pressure, the central corneal thickness will affect the measurement of IOP. Corneal rigidity is the main factor that differs between patients and central corneal thickness is one of the indirect

measures of rigidity. Unfortunately there is no direct measure of rigidity of the cornea in live patients and thus IOP cannot be accurately determined with existing techniques. Studies directed to tonometry strongly recommend not to compare results from patient to patient, but rather use it as a relative determinant of IOP in the same patient, as a precaution [9].

2.2.4 Dr. Asrani's work

Studies have demonstrated that IOP peaks, and most importantly, IOP fluctuations are associated with progression of visual field loss in glaucoma patients even though their office IOP was in the normal range [10]. It is well known that there are circadian variations of the IOP and these fluctuations are more pronounced in glaucoma patients [11]. While the pneumo-tonometry and applanation are the commonly used methods by ophthalmologists and optometrists, making measurements twice to thrice in a year is insufficient to identify the disease early or monitor the disease in its course. Patients with glaucoma are considered "well controlled" if their mean IOP is lower than a certain value (21 mm of Hg). This is based on infrequent measurements over the course of their disease. However, a well known fact is that many glaucoma patients continue to lose vision even when their IOP's are considered "well controlled" due to variations within the acceptable limit. Dr. Asrani (Collaborating Physician in the project) et al [13], after monitoring 105 human eyes with home-use tonometry, reported that, "In patients with glaucoma with office IOP in the "normal" range, large fluctuations in diurnal IOP are a significant risk factor, independent of parameters obtained in the office. Fluctuations in IOP may be important in managing patients with glaucoma. Development of methods to control fluctuations in IOP may be warranted."

Several recent advanced research articles by glaucoma research institutes have comfirmed his view [14] [15].

2.2.5 Intraocular implants for pressure sensing

As continuous monitoring of intraocular pressure has now become important, several groups had then started working towards development of an implantable device that transmits this information continuously or whenever required to an external portable device. The earliest implantable intraocular pressure sensor was developed by Collins [16]. He placed a small passive resonant transensor inside the eye that absorbed energy from an external oscillator at different frequencies depending on the IOP. A more recent fully developed system that is embedded in an intraocular lens was described by Mokwa et al [17]. This device is designed to be implanted following removal of the native lens of the eye. In patients who have not yet developed a cataract, this is a major irreversible surgical procedure in that the patient will end up with an intraocular lens implant just to measure intraocular pressure. Other techniques involve trephining (drilling) the cornea to place a pressure sensor into the anterior chamber. Several research works in implantable pressure transducers have been reported [Michigan, Minnesota [18, 19, and 20]]. The state of the art is possibly best represented by the work of Stangel et.al [17]. They describe an IOP sensor and transponder where the silicon integrated sensor and electronics is implemented in a 2.6 x 2.6 mm die. They also describe a foldable antennae concept but do not propose how it might be built. The long term goal of this project is also to design a relief valve that actuates based on the sensed pressure. Thus the sensor and the actuator together would represent a complete solution for glaucoma treatment. Several other sensors types have been developing including PZT and other capacitor sensors

However, none is available for actual use due to problems of irreversibility (too intrusive). A contact lens based sensor system with a wire coming out of the eye for data transmittance, has been reported in animal models [21]. Having a wire leading out of the eyelids limits its use due to issues of comfort, frequency with which patient has to place and remove the lens and ability of patient to insert the lens. The method is still under refinement and is being developed with wireless telemetry [21]. At present, there is no fully developed intraocular pressure sensor for continuous monitoring.

2.2.6 Drawbacks

As indicated above, the problems that plague the existing devices are:

- **Irreversibility**: The sensor should be easily removable if necessary after the diagnosis or after the management goal has been achieved or if there are any complications due to the presence of the sensor.
- **Intrusiveness and invasiveness**: Sensor insertion, continuous presence and removal if warranted should be minimally invasive and not result in any long term effects on the structure and function of the eye. The device should also control intraocular pressure and should have provision to connect with the drainage tube.
- **Lack of a mechanism to control pressure**: Not much work has been done in controlling pressure based on the sensed pressure
- **High power**: The higher power of the implant poses questions about the safety to the patient in the long run [22].

CHAPTER 3

SYSTEM DESIGN

This chapter describes the design flow that was followed to design the system. The drawbacks of the existing designs were effectively addressed and a better solution is offered. The objective of the chapter is to arrive at a system level design that overcomes the disadvantages of the existing solutions.

3.1 Design Flow

The design of the device was started by first looking into the physiology of the eye and to arrive at the right location for the placement of the implant. This was made possible by Dr. Ramasubramanian working with Dr. Sanjay Asrani of the Duke University Eye Center and carefully mapping the space available inside the eye. It necessitated MRI imaging of the eye and generating a three dimensional volume model of the space available and blocking out the portions not available for the implant. A least intrusive method compared to drilling into the cornea or replacing the intraocular lens with an artificial one was arrived at. The anatomy and size scales for the purposes of this discussion are shown in Figure 3.

3.1.1 Implant Placement

The Space available in the eye for IOP measurement and pressure regulation is very small [Figure 3]. The Thickness of the cornea (Appendix B) is about 500 μm along the optical axis and at the extremities it is about 1 mm. The overall diameter of the lens is about 16 mm.

However, there are axial symmetries inside the eye and if the devices that are built are axisymmetric, they can be radially distributed inside the space available.

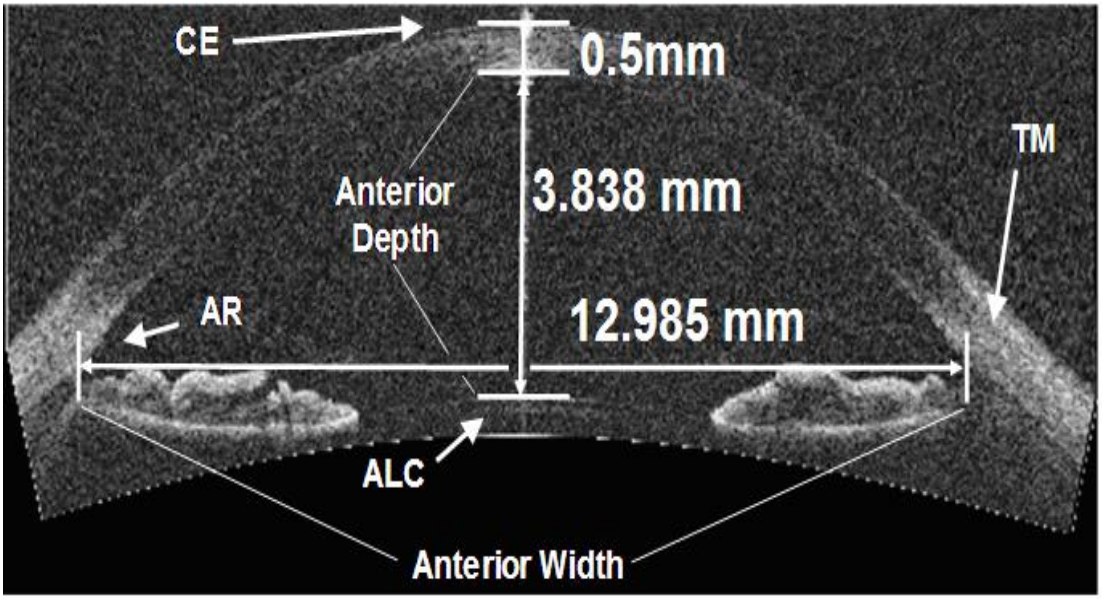

Figure 3. Mapping of the space available in the actual eye by Dr. Asrani.

Courtesy: Picture of original eye taken by Dr. Sanjay Asrani, Duke Eye Center

The selection of the retina surface for the implant is an important aspect of this research. It offers a surface that is easily accessed surgically and the placement of the device like the one proposed is not difficult. The iris is the shutter in the eye and moves rapidly. The maximum movement is near the optical axis and the outer periphery is relatively still, although the muscles do contract somewhat. The motion is entirely radial. Further the anatomy of the iris allows several regions distributed throughout where high density muscular regions are available for device attachment. The volume of the entire anterior chamber can be easily computed treating the chamber as a spherical cap. A cylindrical region along the optical axis must be subtracted out as it is not available for any device placement. In addition to the pressure sensing element, microfluidic channels must be placed in the peripheral region with

valves that are actuated to control the flow. A preliminary examination reveals that the space available in the eye is in the form of a hollow open cylinder, 7 mm ID, 8 mm OD, and a cylinder height of less than 500 micrometers. The flatter the device, better it is for minimal impact on the aqueous humor flow process and the danger of adhering the iris to the cornea. The position of the implant on the iris is shown Figure 4a.

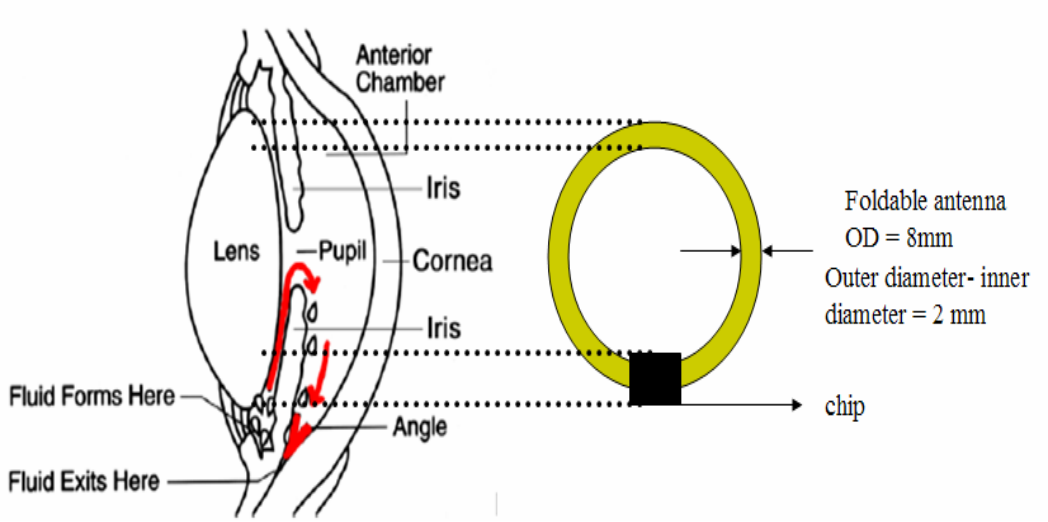

Figure 4a. Dimensions of the implant coil.

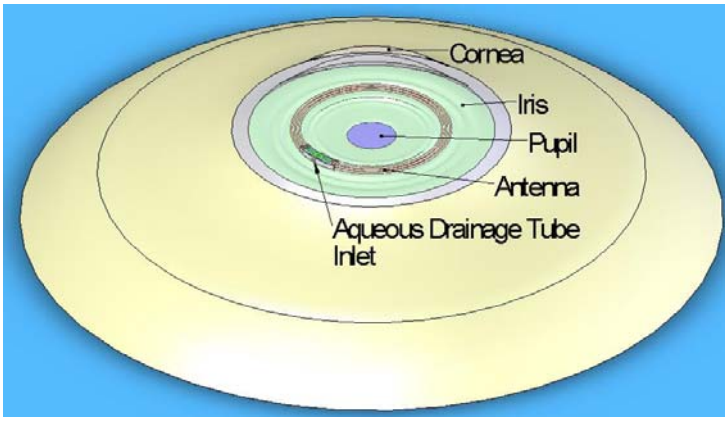

Figure 4b. Position of the implant in aqueous chamber, shown as attached to iris of the eye.

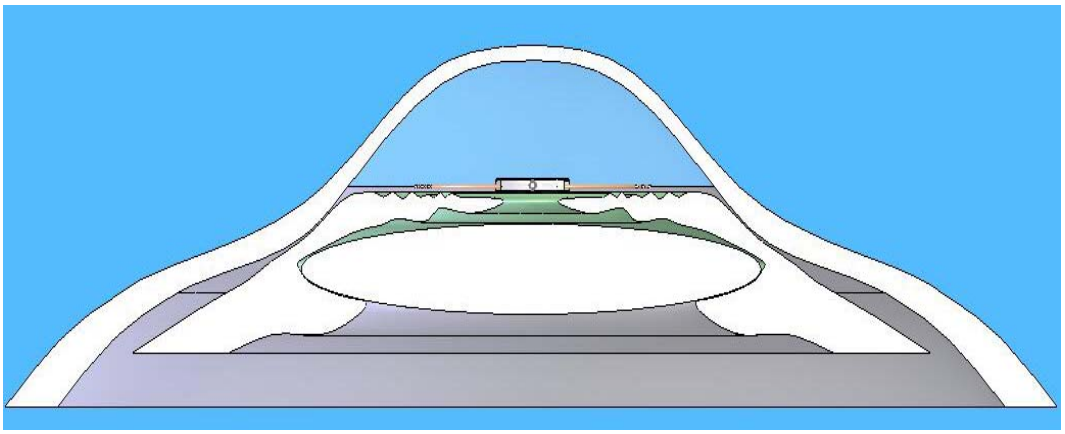

Figure 4c. Side view of the implant in the eye.

Figures 4c and 4d show the side view and cross sectional view of the implant inside the eye. The figures were generated using Solid Works.

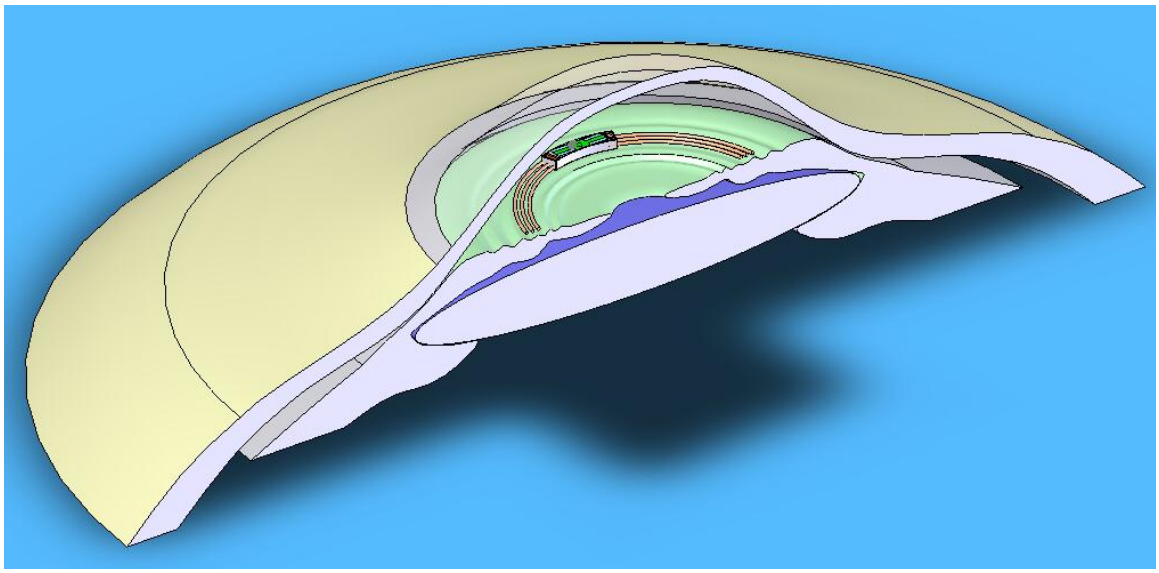

Figure 4d. Cross sectional view of the implant in the eye.

3.2 Structure of the implantable system

The close up of the final design shows a fully integrated device with a silicone coating over it (Figure 5). Packaging of a biomedical implant is very important as it should minimize any fibrous reaction taking place in the patient. The diagram shows a capacitive sensor with a biocompatible top layer, a drainage valve and a provision for the inserting the drainage tube whenever needed. The objective of the design is also to control the pressure when it fluctuates. Hence, the final system also contains the drainage wall which opens or closes based on the feedback signal received from the external device. The drainage tube shunts the ocular fluid to the canal of shlemn and brings down the ocular pressure to the normal level. It also makes sure that the pressure does go down the desired level (Hypotony). The macroscopic antenna is also shown integrated at the bottom of the wafer. The antenna is made of gold which is very much bio compatible and hence does not require a coating over it. The remaining of the device is encapsulated using silicone. The figure shown below shows the location of sensor and actuator in the implant. This research thesis involves the design of the sensor part alone and not the actuator valve.

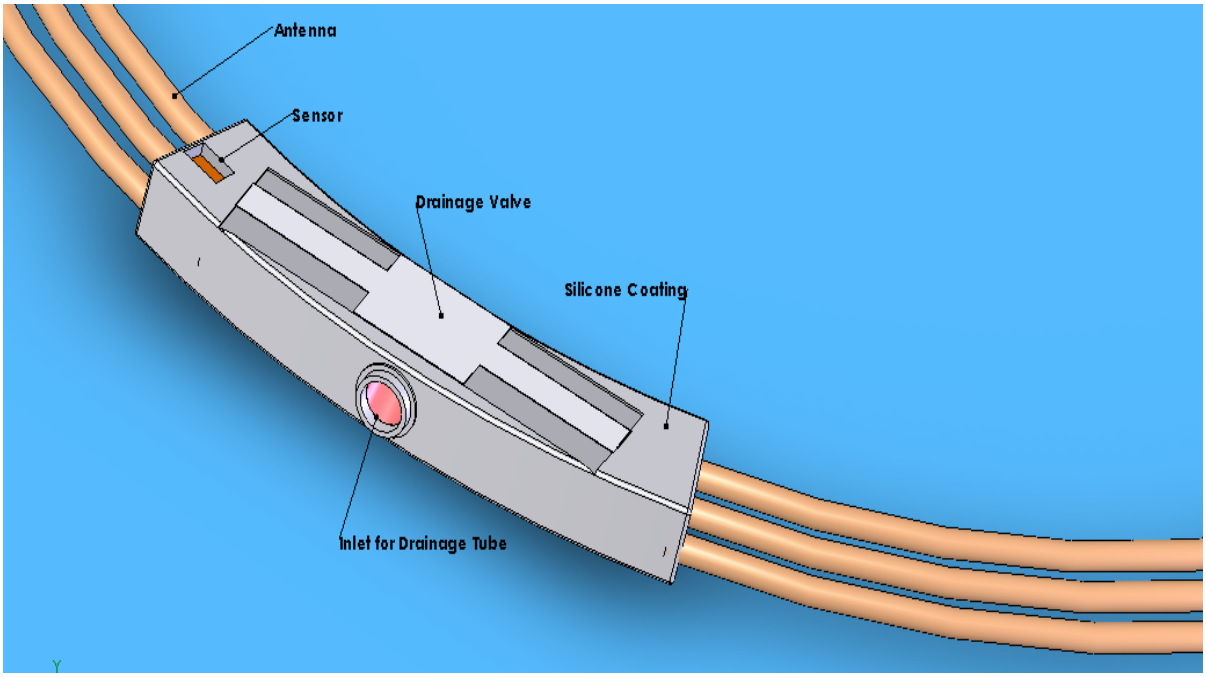

Figure 5. Fully integrated and packaged implant with biocompatible silicone coating and opening for the sensor and an inlet for drainage tube.

3.3 Why MEMS, and post CMOS is preferred and not an intra CMOS process?

The above design was planned to be implemented by solder bumping the CMOS circuitry with the antenna and the sensor. The MEMS structures that are to be integrated with the device include the sensor, valve and the antenna. As the valve requires use of special materials it cannot be fabricated in a conventional CMOS process and moreover intra CMOS fabrication of the MEMS structure is not possible as interference with a conventional fabrication flow to fabricate the MEMS part of the device is not possible. Hence Post CMOS integration i.e integration of the CMOS circuitry with separately formed MEMS microstructures is the only available solution. Another advantage of this strategy is that making a complete device in a single wafer would consume lot of real estate due to the

macroscopic antenna. Use of wound microcoils instead of surface micromachined coils for the implant antenna will also be explored.

CHAPTER 4

WIRELESS INDUCTIVE LINK DESIGN

An important subsystem in the above device is the antenna subsystem which comprises of an implant coil and an external transmitter coil. The objective of this section is to arrive at optimum dimensions for the antenna coil.

4.1 Inductive power Link

Systems must be designed for use with wireless power and data transmission. The wireless power transmission is implemented in practice through the use of an inductive link which is basically a weakly coupled coreless transformer. Power supply for the sensor system is obtained by rectification and filtering of the received radio frequency signal. The low power efficiency of this link is one of the main driving forces for low power design in inductively coupled sensor systems.

4.1.1 Power Losses in the system

The power dissipation or loss can be regarded as taking place in three locations, the transmitted power stage, the link and inside the implant. The unfocussed power transfer and the weak coupling of parts lead to very low link efficiency. Hence the task of the transmitter is to set up at the location of the implant, a magnetic field which is strong enough to power the implant.

4.1.2 Simultaneous Control data Transmission with power

Digital control data transmission to the sensor is made possible by modulating the RF carrier signal and reverse transmission can be implemented by varying the load seen by the secondary of the transformer. This type of load shift keying is only possible if the coupling in the transformer is large enough. The other method of reverse transmission is by ON/OFF transmission of a constant RF signal. The period of the ON/OFF portion of the signal contains information to be sensed. In the current design, a very simple control is required which controls the operation of the device in one of the two modes i.e sensing mode and calibration mode which will be discussed in the next chapter.

4.1.3 Problems associated with Load Shift Keying.

The weak coupling between the primary and secondary makes the load provided by the implant on the transmitter side quite insignificant. The requirement for this mode of data transfer is short distance between the transmitter and the implant which is not very much suitable to our application. Most of the reported work which uses load shift keying uses shallow implants such as transcutaneous implant. The design goal is to maximize the transferred power subject to limitations in the size and quality of the implanted coil. So, a wide range of materials have to be explored in the construction of implanted coils. The existing work in implants have used hardwound coppers to on-chip planar spiral coils made with standard materials, some use Pt apart from Au due to its more inert nature.

4.2 Performance specifications of the link:

Performance specifications of the link like power transfer, range and bandwidth are best calculated using a circuit-level description of the link. However there are a few circuit elements which can be described only using physical description of the system such as inductance of the coils and mutual inductance or coupling coefficient. Inductances can be calculated using analytical approximations or using semi empirical models from simple coil geometries. There are few field simulator tools such as Fast Henry of Fast field solvers and MemHenry of Coventorware that help in calculating these parameters for even complex geometries. For operating frequencies in the order of 10 MHz and with dimensions larger than in RF on-chip inductors, the losses are mostly due to bulk resistance and current crowding in the conductors.

4.3 Range and Power transfer

The range of the link is closely connected to the power transfer since the range is the distance at which the transferred power falls below the requirement of the implant. The power transfer is a strong function of distance, so the range is constant regardless of the power consumption of the implant. An expression for range can be calculated based on this premise. There are two main factors which contribute to the difficulty in the determination of power transfer. One is the complex dependence of mutual inductance on geometrical details and the other is the non linearity in the power converter. The method followed was to use a field simulator to obtain mutual inductance and then use a circuit simulator to calculate power transfer.

4.4 Circuit level Description of the link:

The behavior of the inductive link between the external and internal circuitry can be treated at two different abstraction levels [23], the electromagnetic field description and at the circuit level. The electromagnetic description is based on the geometry and physical composition of the link elements, but does not give direct information about the way in which electrical signals propagate through the transmission channel implemented by the link. The circuit level description on the other hand can be used to derive channel characteristics, but key parameters of the circuit elements like inductances, parasitics and coupling coefficients can only be extracted from the electromagnetic field description.

4.4.1 Circuit level description -Transformer model

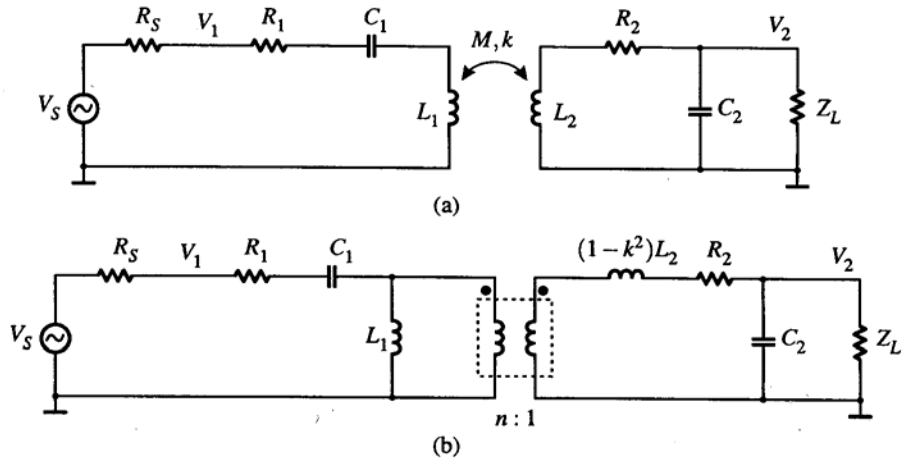

Figure 6. A linear model of the weakly coupled inductive link. (a) Weakly coupled inductive link, (b) shows an equivalent ideal transformer with two uncoupled inductors replacing the weakly coupled transformer.

Ref: CMOS circuit design for RF sensors.

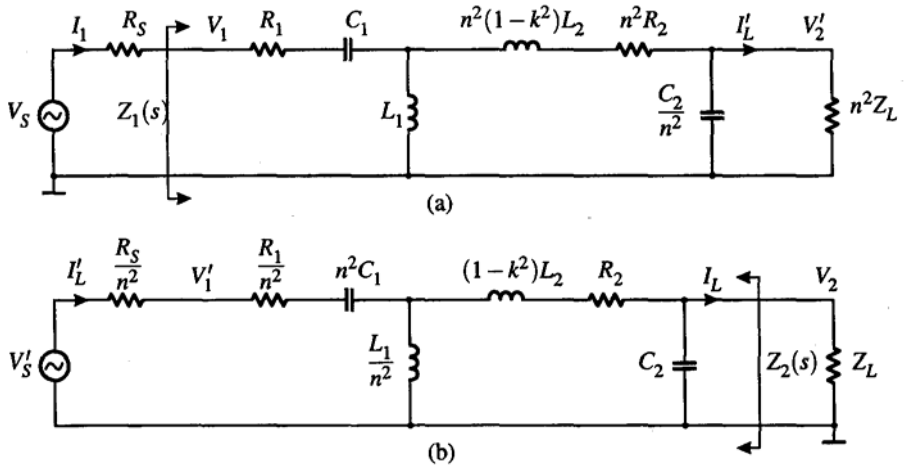

Figure 7. A linear model of the weakly coupled inductive link. (a) Link circuit referred to the primary side (b) link circuit referred to the secondary circuit.

Ref: CMOS circuit design for RF sensors

The link can be treated similar to a lossy, weakly coupled transformer [23]. The contributions to the losses in the transformer stem from the series resistances in the inductors, while core losses are of course absent. The link inductors are tuned to the operating frequency for better efficiency. The primary circuit in most cases tuned in series to provide a low impedance load to the driving transmitter at the resonant frequency. The secondary on the other hand is a parallel LC circuit to better drive a non linear rectifier load. The high output impedance of the parallel circuit is the best match for a rectifying power conversion circuit, which for all practical purposes looks like a rectifier connected to a stiff voltage source.

Figure 6 above shows a working model of the transformer or in other words, the link with parasitic resistances of the inductors shown as R_1 and R_2. R_S is the source resistance. C_1 and C_2 are the parasitic capacitances of the primary and secondary coils respectively. When the secondary circuit is analyzed as an isolated circuit it can be useful to transform the series

resistance into an equivalent parallel resistor with a simple series to parallel transformation.Q_2 is the transformation coefficient.

$R_{2p} = Q_2^2 R_{2s}$ - 1

The mutual inductance is a physical parameter which depends on the geometry of the link, while the coupling coefficient is a circuit parameter used to describe the effect of the mutual inductance in the circuit abstraction. The relation between the two is given by

$M = k\sqrt{L_1 L_2}$ - 2

Where M is the mutual inductance and L_1 and L_2 are the self inductances of the primary and secondary coil. The characteristics of the link can be observed from two points of view. At the primary side, the input impedance defines the drive requirements for the transmitter. An analytic expression for the input impedance also shows the effect of the secondary circuit on the primary, and can be used to gauge the observability of load variations in the secondary circuit. This can tell us whether load modulation is a practical proposition for outbound data transfer for a given link coupling. The properties of the link seen from the secondary side are useful to calculate the power transfer and the transmission channel characteristics for inbound data [23].

4.5 Transfer Functions

The equivalent circuit with the weakly coupled transformer can be redrawn as a circuit with ideal transformer. This circuit can be used to derive expressions for the most interesting link performance parameters namely the power or current transferred to the load, the output requirement for the signal source, the bandwidth of the link and the sensitivity of the primary input impedance on the secondary load. These double tuned links have a fourth order band

pass transfer function with two pairs of complex conjugate poles [23]. The load seen by the signal source can be derived. The dependence of this impedance function on the secondary load is required to determine the observability of load variations at the transmitter. If the load resistance is modulated between two values R_{L0} and R_{L1}, the modulation index of the inductor voltage is given by

$$m = \left| \frac{V_{L0}(R_{L0}) - V_{L1}(R_{L1})}{V_{L0}(R_{L0}) + V_{L1}(R_{L1})} \right| = \omega^2 k^2 L_1 C_2 \left| \frac{(R_{L0}) - (R_{L1})}{(R_{L0}) + (R_{L1})} \right| \quad - \quad 3$$

This is a useful expression [23] because it tells us that the maximum voltage modulation index perceived across the primary inductor $m_{\max} = \omega^2 k^2 L_1 C_2$. The inductances in the primary and secondary are usually similar, while the secondary inductor may have a smaller diameter it is often practical to use more turns in the secondary. The assumption L_1 and L_2 are equal leads to the result that the maximum modulation index is equal to the coupling coefficient squared. The source impedance seen by the secondary load influences the design of the power conversion circuit. The exact expression of the source impedance can also be derived. In the final source impedance expression we can neglect the effect of primary completely and only take the secondary passive circuit elements. The source impedance is mainly affected by the nearside of the link and the effects of the far side of the link are secondary and negligible. The impedance is thus of a simple RLC circuit.

From this impedance voltage transfer function at the resonant frequency can be obtained between source voltage V_s and Voltage at secondary output V_2

$$A(\omega_0) = \frac{V_2}{V_s} = \left[\left(\frac{k(R_{2p} \parallel R_L)}{(R_1 + R_s)} \right) \sqrt{\frac{C_2}{C_1}} \right] \qquad - 4$$

4.6 Range:

The procedure to find range is to find k at which the link gain reaches the input threshold of the power converter, and subsequently translating this coupling coefficient to a physical distance using the methods in the next section. The converter threshold is a function of two variables, the internal supply voltage (V_{dd}) implant and the voltage drop V_D in the converter. The voltage drop depends on the converter topology and is roughly two rectifier drop for most other types. If we assume that the range is determined by the k for which the secondary voltage reaches the converter threshold $V_2 = V_D + V_{dd}$. The design takes this voltage V_2 as 3.3 V and calculates the coupling coefficient. By approximating the resistances in the primary and secondary to be same and taking C_2 as 10 times C_1 we get K as 0.15 for a transmitter supply voltage $(V_s)_{of}$ 12V.

$$k = \frac{(|V_D| + Vdd)(R_1 + R_s)}{V_s R_{2p}} \sqrt{\frac{C_1}{C_2}} \qquad - 5$$

This is the minimum coupling coefficient needed to provide the full supply voltage for the implant.

4.7 Electromagnetic model to find Mutual Inductance:

The magnetic field created by a current flowing through a coil of radius a at a distance r is given by

$$B = \frac{\mu_0 I a^2}{2(a^2 + r^2)^{3/2}} \qquad - 6$$

This magnetic field is directed along the axis. The $1/r^3$ dependence is precisely the reason why the range of the inductive links is limited. The potential U induced in a secondary circuit due to a time varying magnetic field is given by

$$U = -\frac{d}{dt}\int_S B.du \qquad \text{- 7}$$

Where S is any surface linking the circuit and u is the unit vector normal to the surface. The magnetic field from a circular current loop can be calculated at an arbitrary point but this leads to elliptical integrals which must be evaluated numerically. The regions around the loop can be distinctly classified as near field (r<<a) and far field (r>>a). All inductive links operate as near field antennas as the characteristic dimensions are mush smaller than the operating wavelength. However, a measure of radiated power must be made so that it is compliant with local frequency spectrum regulation. The goal of the preceding field calculations was to find a starting point in the evaluation of the effects of geometry on the coupling constant between the primary and secondary antenna. If we assume that the two current loops are approximately coaxial and parallel, meaning that the axial shift is small compared to the separation. Further, the angle spanned by the secondary seen from the primary is small or equivalently that the diameter of the secondary is small compared to the separation, we obtain the flux φ by multiplying the field by the area. One definition of the mutual inductance of two loops is the flux through one divided by the current in the other, we have

$$M_{12} = \frac{\mu_o \pi N_1 N_2 a_1^{\,2} a_2^{\,2}}{2\left(a_1^{\,2} + d^2\right)^{3/2}} \qquad \text{- 8}$$

The mutual inductance and the coupling coefficient are related by $k = M\sqrt{L_1 L_2}$

Figure 8a shows the link simulates in Fast Henry to extract frequency dependent mutual inductance.

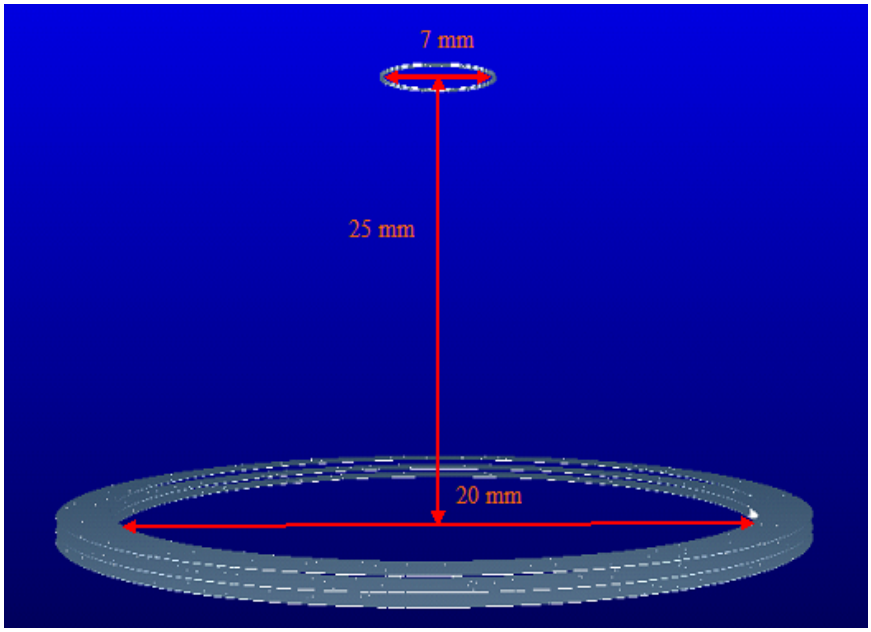

Figure 8a. Primary and secondary coil created using MemHenry.

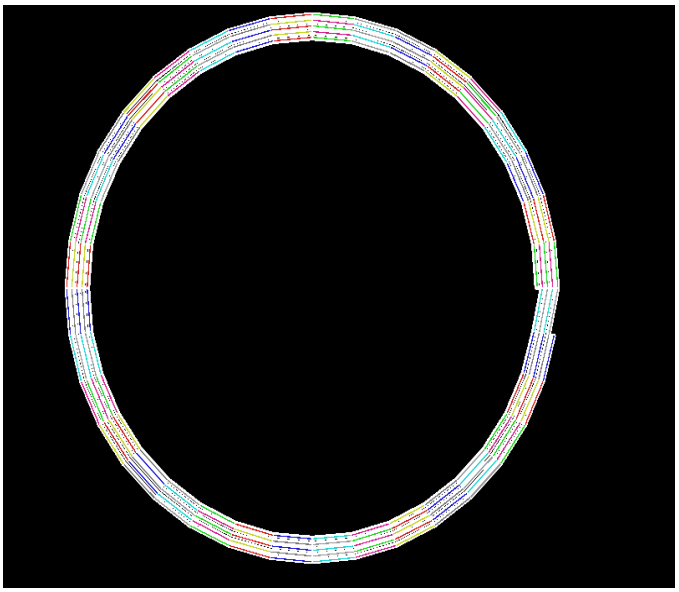

Figure 8b. Secondary coil zoomed in with 4 turns and a single layer created using MemHenry. (Dimensions 8mm OD, 7 mm ID, 50 um thick and 100 um height)

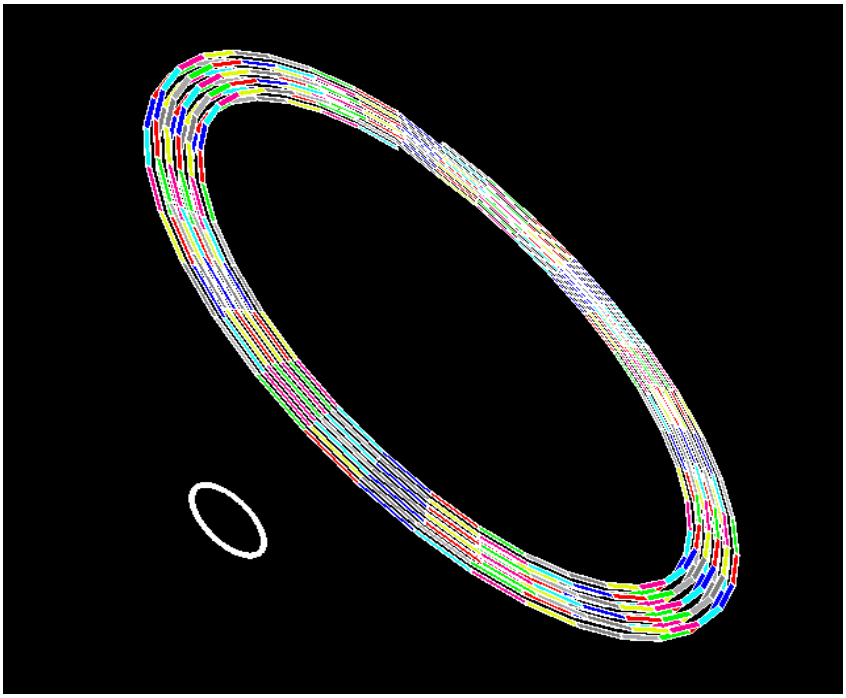

Figure 8c. External transmitter coil and implant coil. (side view)

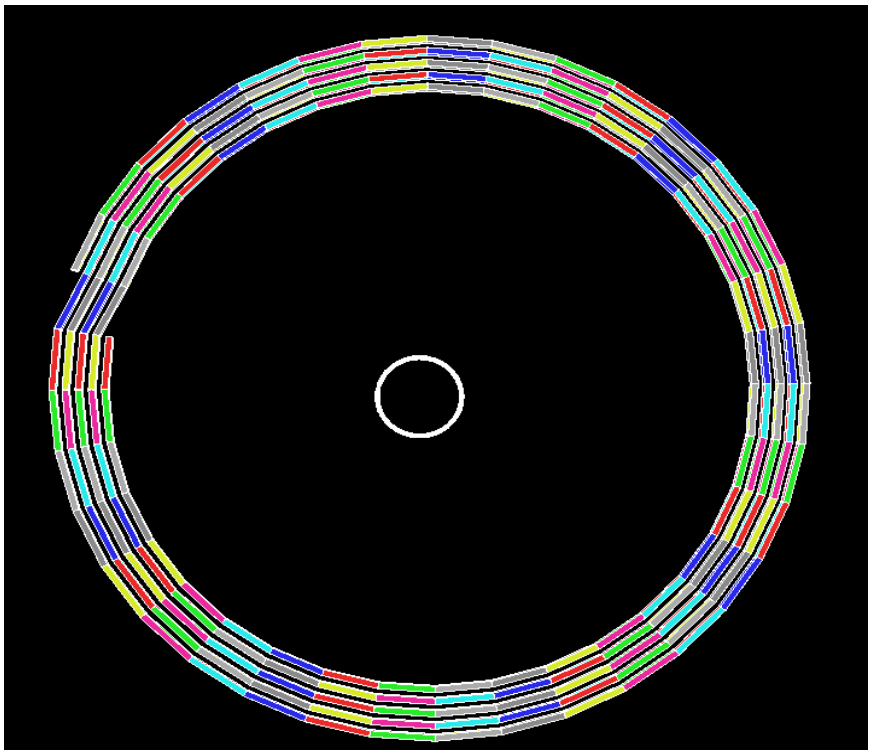

Figure 8d. External transmitter coil and implant coil. (x-y plane)

4.8 Frequency selection:

FCC has allocated certain frequencies which are royalty free for Industrial, Medical and scientific operation. The frequencies are 125 KHz, 13.56 MHz , 800 MHz and 2.4 GHz. For inductive power links, near field power transmission is important which increases with frequency. However high frequency electromagnetic waves are partly absorbed by the tissues in the body. The frequency range of operation considering trade off between tissue absorption, power transmission and maximum data bandwidth is 10-20 MHz. In our application the bandwidth is not a concern however, inorder to operate in the royalty free dedicated ISM (Industry scientific and Medicine) 13.56 MHz was chosen. Any frequency below 10 MHz can also be selected but the values of inductor and capacitor to operate at low frequencies would be large and hence would require more area. Figures 9a and 9b show the effect of frequency in coil resistance and inductance.

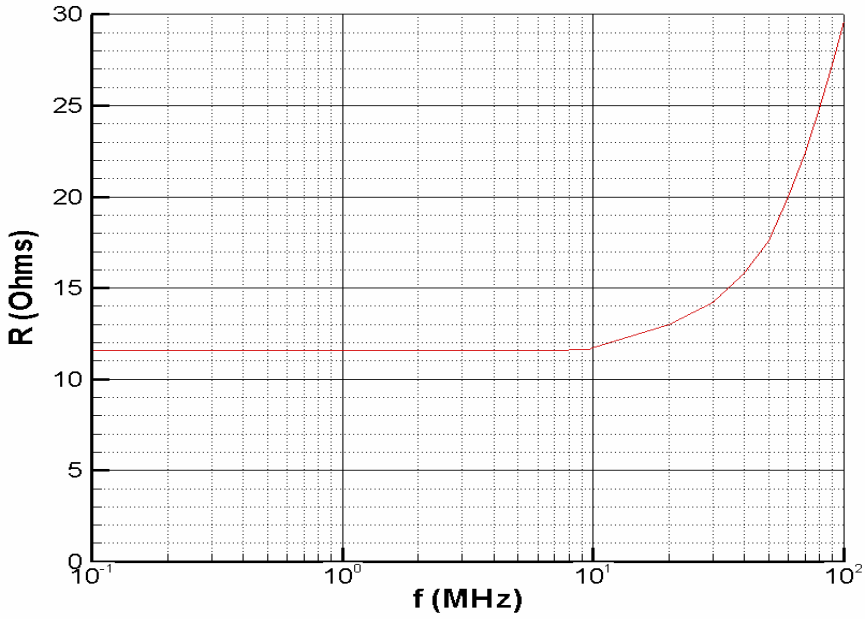

Figure 9a. Large increase in resistance of the secondary coil due to skin effect.

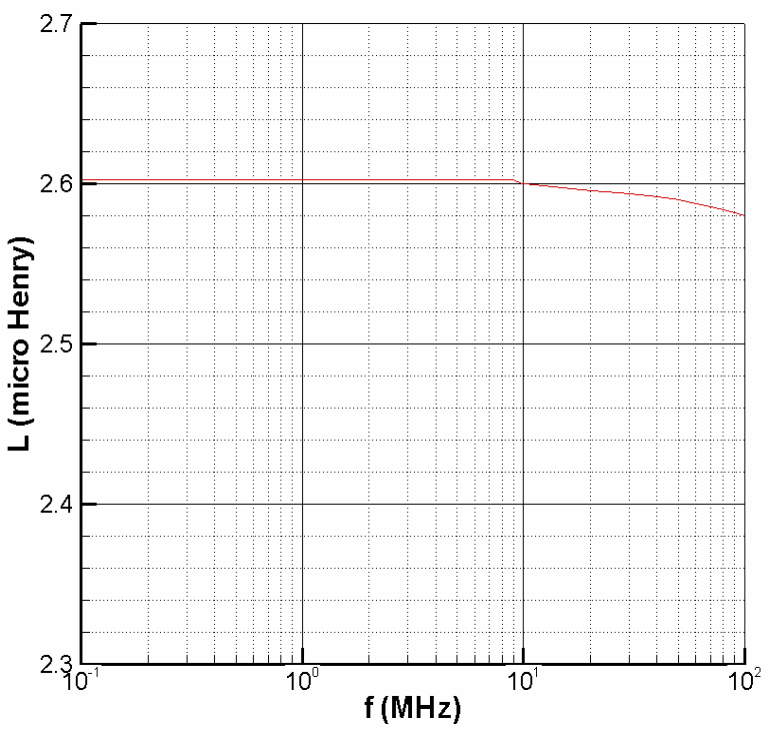

Figure 9b. Small reduction in inductance with frequency.

4.9 Effect of coupling coefficient on Range

From the extracted mutual inductance using field solver tools, the coupling coefficient is calculated. The variation of the coupling coefficient with distance between coils is shown in Figure 10a. The figure has curves for different radii of the primary coil. For each of these curves, the range is limited at the point where the coupling coefficient reaches 0.15. There are several ways of improving the range like increasing the transmitter power, changing the dimensions of the secondary and primary to increase mutual inductance. In the next section it has been observed that increasing the number of turns in the secondary does not affect its inductances much except that it increases its series resistance and brings down the quality factor of the circuit.

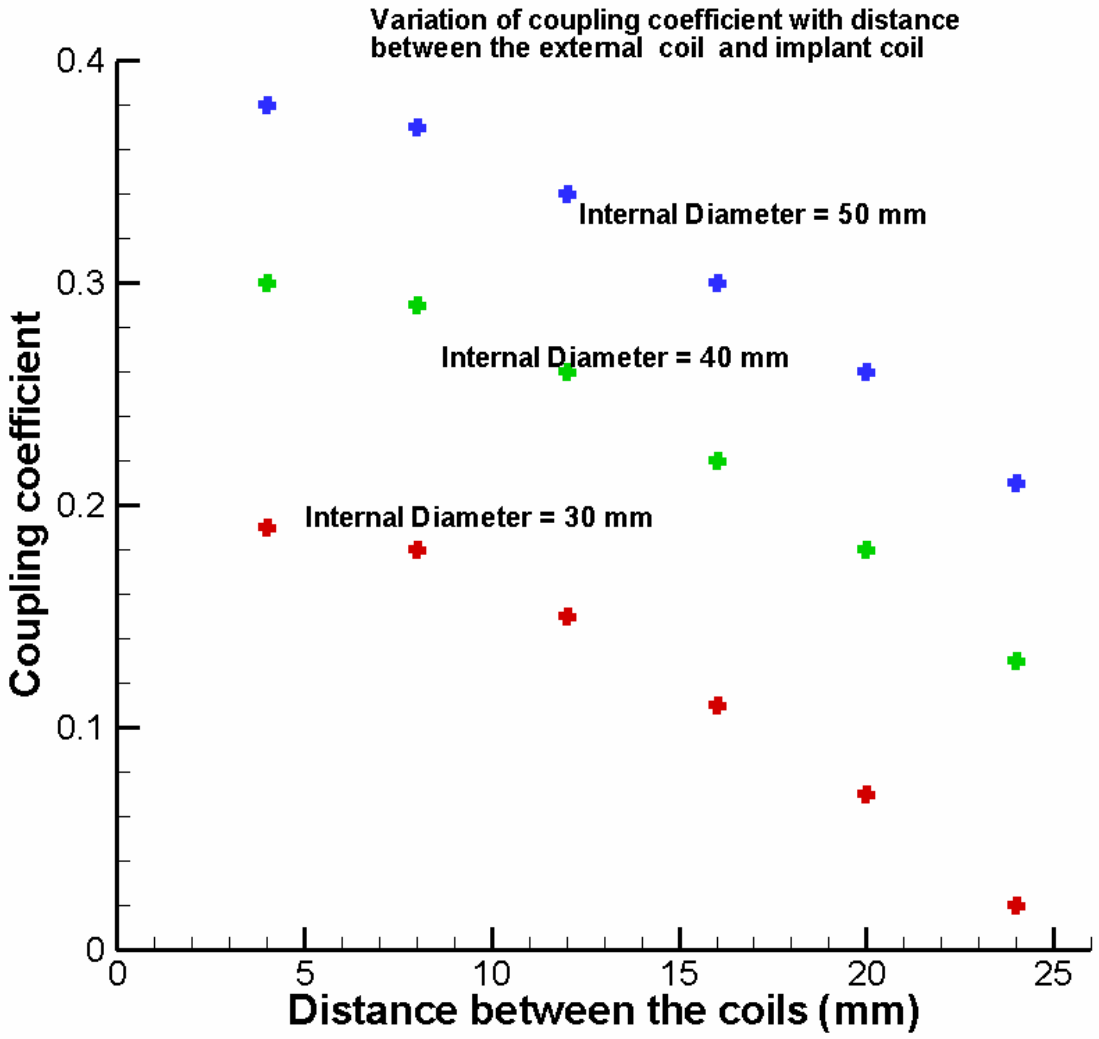

Figure 10a. Figure indicating coupling between primary and secondary coil increasing with smaller distance (z) between the coils, plots for various values of internal diameter of the primary coil are shown.

4.10 Parasitic capacitance of the secondary coil

In order to improve mutual inductance, the distance between the coils of an inductor cannot be reduced rigorously to accommodate more number of turns. This is due to the adverse

effect of parasitic capacitance between the coils. The parasitic capacitance forms a parallel capacitor to the sensing capacitance. Hence, the parasitic capacitance has to be very much reduced.

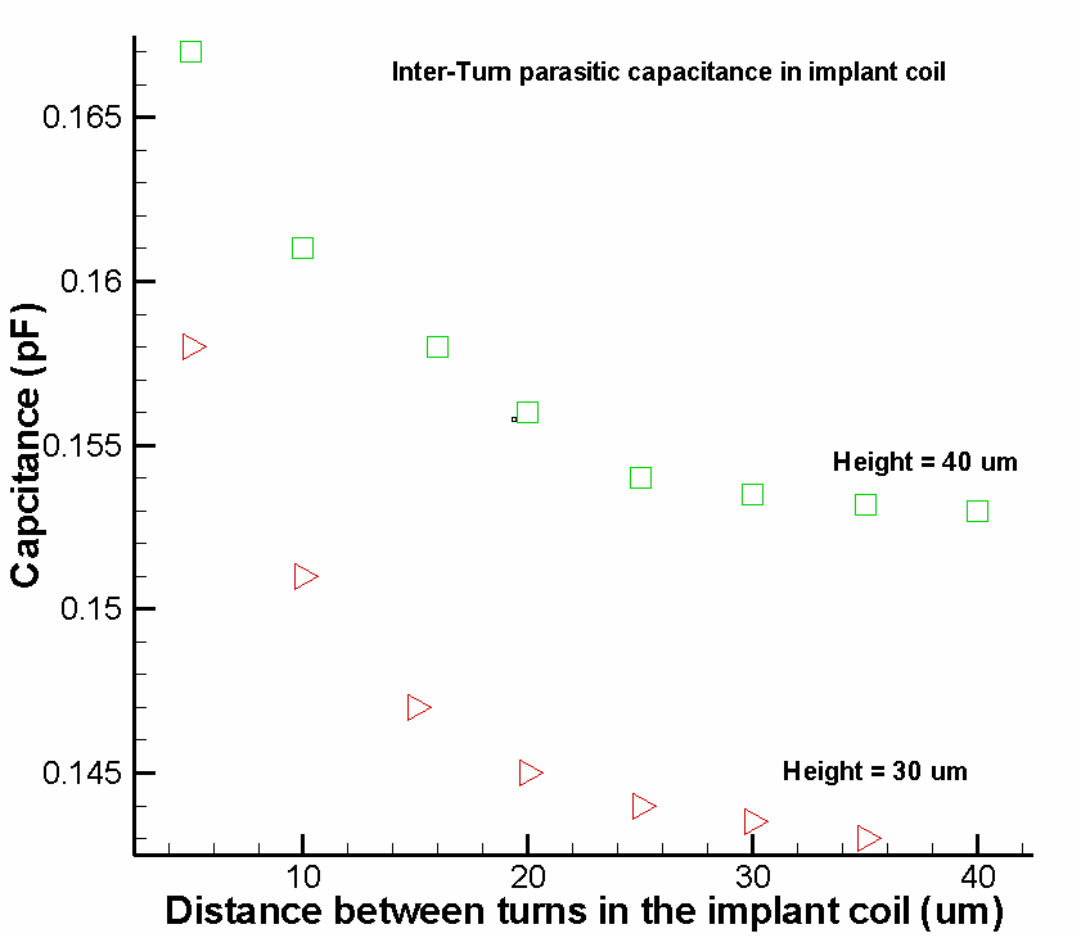

Figure 10b. Figure indicating the increase in parasitic capacitance with decrease in distance between turns caused due to increase in the number of turns in the available space. Plots for various values of height of the implant coil are shown.

4.11 Physical dimensions of secondary coil

The secondary coil can have radius ranging from 3.5 mm to 4mm. The trade off in selecting

the secondary coil dimensions (width, and height) is trade-off between series resistance and self inductance. Increasing the number of turns increases its inductance but also increases the series resistance associated with the inductor, hence losses. The change in net inductance as seen from the input side was almost constant with the change in dimensions of secondary. Hence not much benefit is gained by increasing the secondary coil turns by few numbers (Figure 10c). The insignificant change in inductance seen from the primary coil side is due to large primary inductor value compared to the secondary coil.

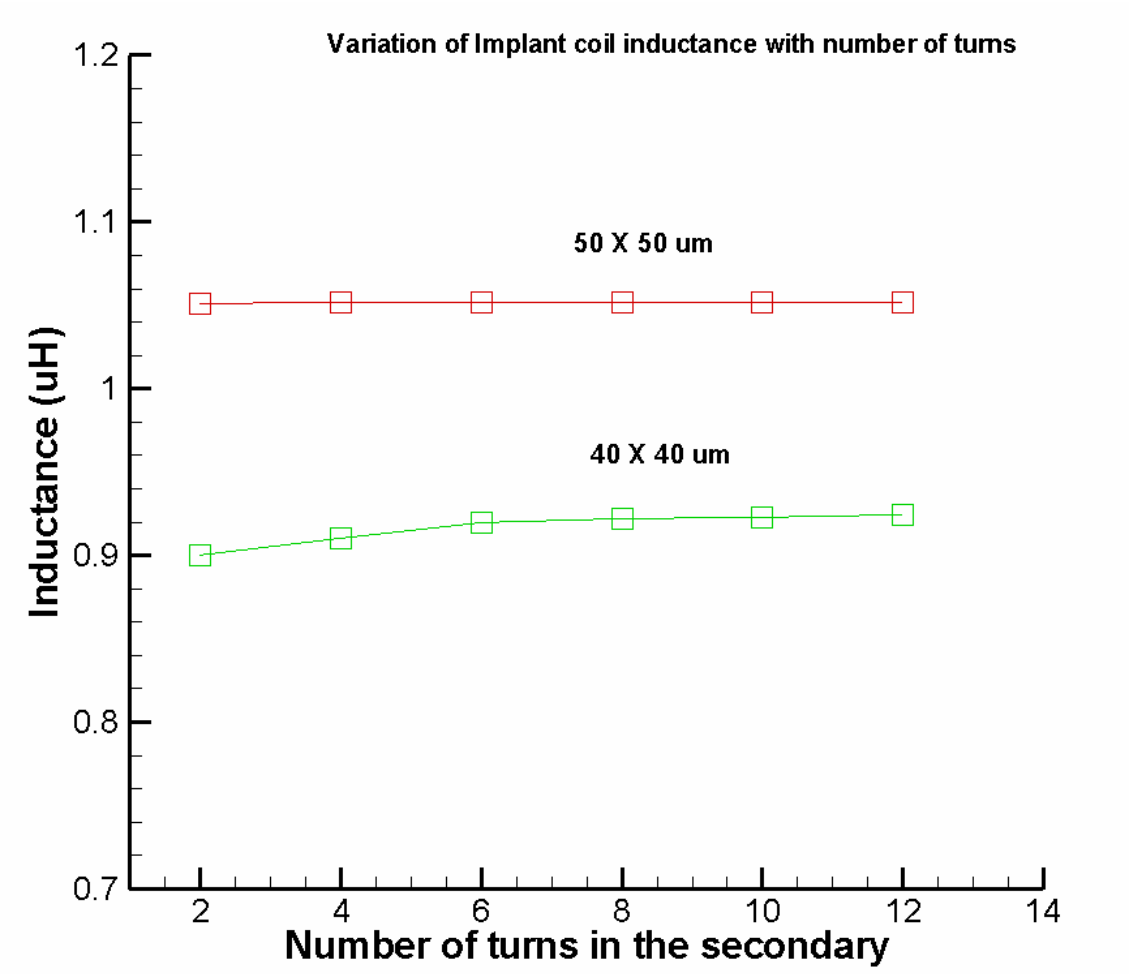

Figure 10c. Figure indicating the insignificant change in net inductance seen from primary coil.

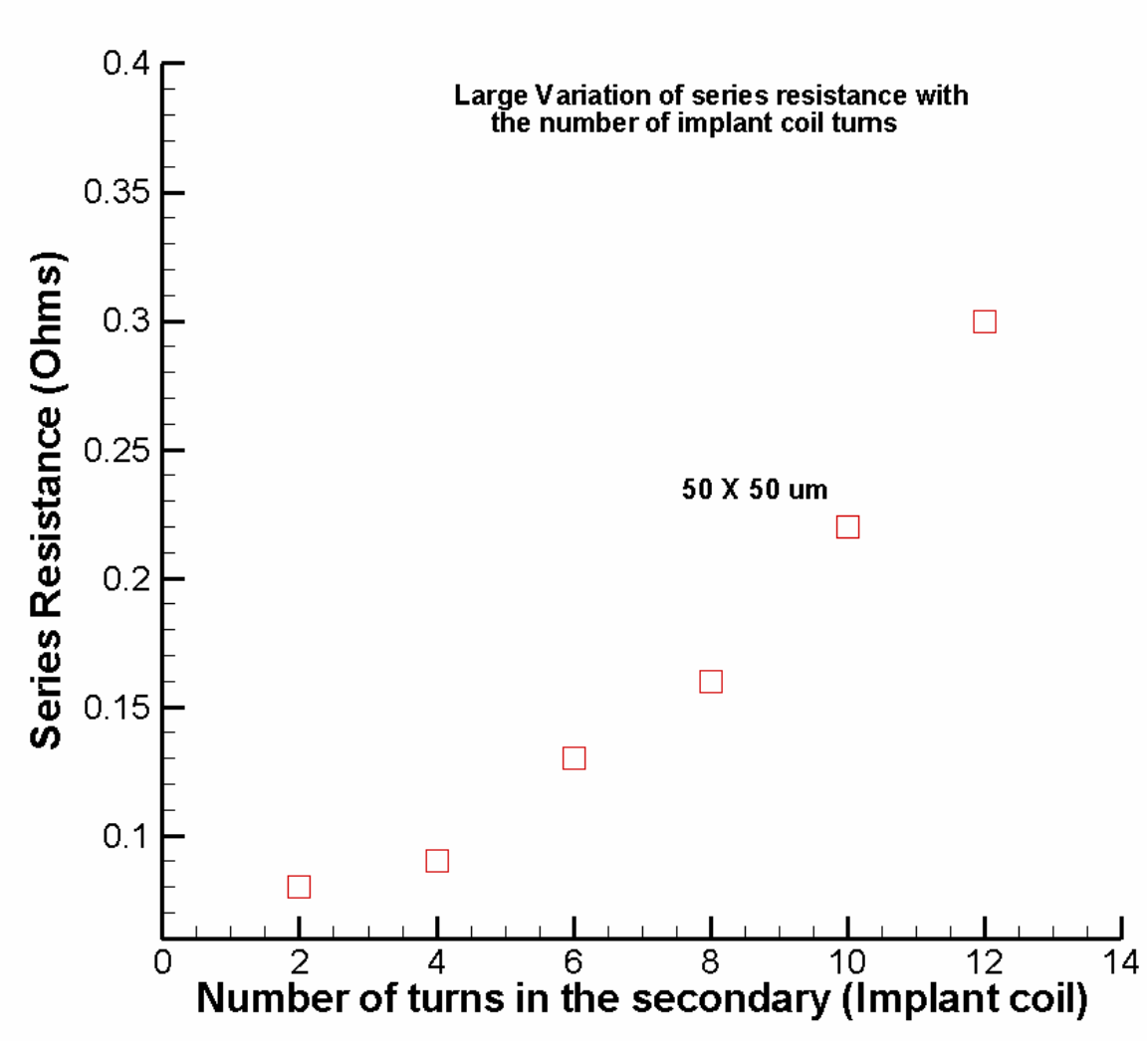

Figure 10d. Plot of series resistance of inductor with number of turns.

The above two curves indicate increasing the number of turns in secondary is not efficient as it reduces the Q of the circuit by increasing the net resistance. The above observation is due reduction of width of the secondary coil to accommodate more number of turns which results in increase in its resistance. Hence due to insignicant impact of the secondary turns on net mutual inductance, the number of turns was chosen to be 5 with the objective of reducing series resistance. This corresponds to 50um coil width, 30 um spacing between turns. Single layer of coil can be accommodated with coil height as 100um.

4.12 Physical dimensions of Primary Coil

Significant increase in coupling coefficient will take place only if the number of turns in primary is increased and/or radius of primary coil is increased. The simulation was conducted for different distances of the primary coil from the secondary coil and was shown earlier.

Thus from the above graphs, distance between the primary and secondary coil was chosen to be 25 mm (It is roughly the distance between human lens and center of external spectacles to which transmitter antenna can be attached.). The radius of the primary coil chosen was 25-35mm. This is limited by the space constraint. As expected the coupling increases with the number of primary coil turns. The number of turns in the primary chosen was 5. The width of the primary coil was chosen to be 2 mm and the distance between the turns as 1mm. Optimal coupling was observed with ratio of outer and inner diameter of primary coil close to 3.33. The value of the net inductance arrived for the above dimension of primary is close to 1uH. This can be easily increased by increasing the primary coil turns and its area of cross-section. The above values were chosen after observing minimum series resistance in the simulation and there is still scope of improving the coupling which could be explored after exact range of sensing capacitances is arrived.

4.13 Conclusion

Thus from the analysis made in section 4.9 through 4.12, the following final design of the antenna is arrived at.

4.13.1 Final Design of the Antenna

The antenna subsystem consists of a planar, primary transmitter coil with a single layer of turns. The number of turns in the primary coil is chosen as 5 based on the analysis. The

number of turns and the number of layers of the primary transmitter coil can be varied. The secondary coil is a single layered, multi turned planar coil fabricated on chip. As discussed in the above sections, the design of the secondary or implant coil has severe space restrictions. The inner and outer diameter of the coil is fixed as indicated in the section 3.1.1. The only way of increasing coupling is through increased number of turns. Figure 10c shows precisely the effect of increasing the number of turns. For the chosen primary coil dimensions, the implant coil dimensions are reduced until the parasitic resistance of the coil does not increase alarmingly. Thus for this design, the final dimensions arrived at the end of the analysis are

- Secondary coil dimensions: coil width =50um, coil height= 100um, spacing between turns =30um, with a single layer.
- No of turns of secondary coil turns = 5
- Primary coil dimensions: width =2mm, height = 1mm spacing =1mm

  Outer radius = 25 mm, inner radius for max coupling = 8.5 mm
- No of turns of primary coil turns (can be changed) = 5

4.13.3 Performance of the Antenna

The antenna design proposed results in a coupling coefficient of 0.15 and a range of 2.5 cm. The Voltage induced in the secondary coil at this range is 3.3 V. Thus, the antenna design has attained the required specifications (see section 4.6). However, the induced voltage, coupling coefficient and the range can be improved from the above obtained values by increasing the transmitter voltage, number of turns in the primary coil, the layers in the primary coil and/or radius of the primary coil.

CHAPTER 5

POWER AND CONTROL CIRCUIT DESIGN

This chapter deals with the design of the control circuitry along with power conversion and conditioning circuits. The process chosen was AMI 1.5 um process. The maximum supply voltage for this process is 3 V. As seen in chapter 2, the major objective of this design is to achieve low power and reliable operation of the device.

5. 1 System Block Diagram

A simple circuit design would help in reducing the power dissipation. The following section describes a system which uses a simple mechanism of charging and discharging the sensing capacitor to generate a signal proportional to the pressure inside the eye.

5.1.1 Function

The capacitor when charged with a constant current source produces a saw tooth waveform. This capacitor voltage is compared to a reference and the comparator will produce pulses which will also discharge the capacitor at every cycle through a strong pull down network (Figure 11). After the output of the comparator switches off, it will discharge the capacitor after a small delay to set up the pulses for the comparator circuit which is then fed to the ring oscillator. These pulses are gated with an RF signal and will be transmitted to an external receiver via a wireless link. There is an on-chip calibration capacitor which will be used to obtain a correlation factor of frequency and pressure at the beginning of every measurement. The calibration capacitor on the chip will be charged with a current source and compared to

the band gap reference to ensure that pulses are at known frequency and that will define our correlation factor between pulse frequency and eye pressure. Then it will switch to an external measurement capacitor whose fabrication will be discussed in the next chapter. When the measurement capacitor is switched to the comparator the frequency readings will define actual measurement of eye pressure using the value of correlation factor obtained. Figure 11 shows the block diagram of the system.

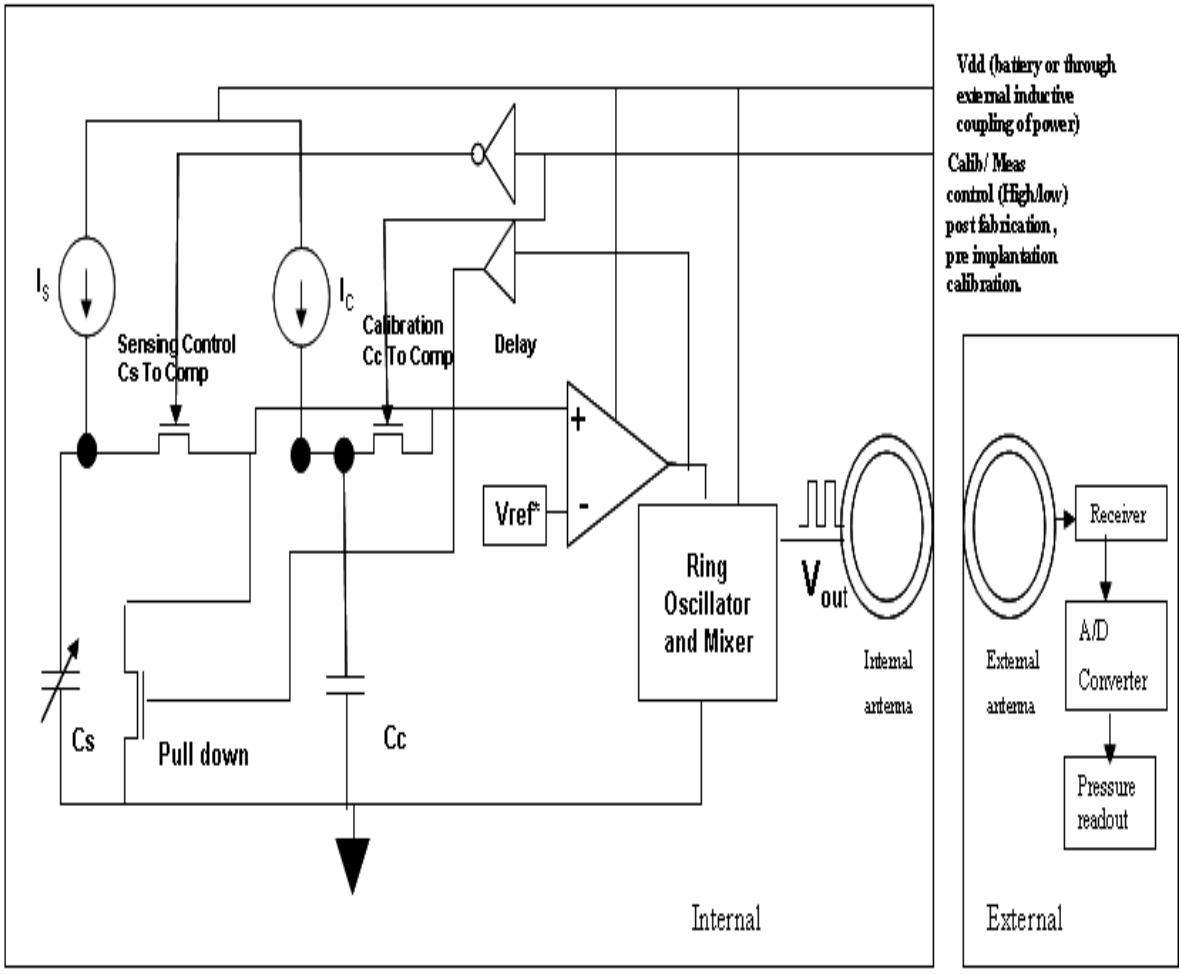

Figure 11. Block Diagram of control circuit in the system.

Figure 11 shows the complete block diagram of the system. The various components that can be seen are

- Cc -on Chip Poly Capacitor Cc to be used for calibration
- Cs-sensor capacitor
- Ic, Is - Current source for charging, calibration of sensor capacitors.
- Band Gap reference circuit
- Comparator
- Inverters
- Switching FETs
- Ring Oscillator and mixer

5.1.2 Detailed description of the circuitry in the system:

Sensing capacitance functionality: Sensing capacitor Cs will be charged by the current source shown in Figure 11 and will create a ramp signal that will be compared to a level Vref. The comparator will send out pulses at a frequency proportional to the capacitance Cs.

Calibration capacitance: Cc is a calibration capacitance and it will be used at first to ensure that detector is reading correct data and if there is a small variation in body temperature the calibration cap will help the receiving end to detect that and adjust scaling level.

Switch: It is a switching FET Controlled by Cal/Meas pin which will be High at calibration and Low at measurement. This control signal can be wirelessly transmitted by embedding it in the power signal.

Reference voltage: Both Ic and Is will be mirrored to a reference current that is controlled by a band gap reference voltage.

Ring Oscillator: For the RF output, a voltage controlled ring oscillator can be used to generate an amplitude-shift keying signal.

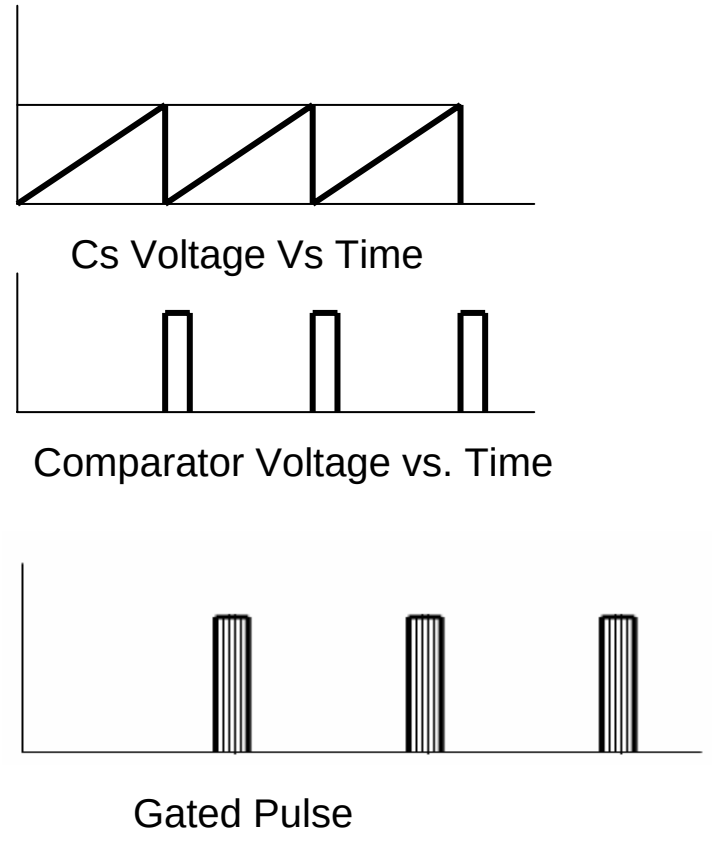

Figure 12. Signals generated in the circuit.

Calibration circuit:

When the circuit starts, MOSFET CcToComp connected to calibration capacitor is switched ON and connects Cc to the comparator. The frequency of pulses measured during the calibration is used as a benchmark to interpret the frequency of pulses obtained during sensing.

Measurement circuit:

When Cal/Meas signal is lifted low CsToComp FET will turn ON and CcToComp FET will turn OFF. The measurement capacitor charges and discharges at a rate proportional to the capacitance value and to the pressure on the capacitor.

Chip signals:

- Vdd, the chip power source
- GND
- Meas/Cal this signal will be held low at calibration and High at measurement
- MeasCap, Since measurement cap is not implemented on the chip
- PulseOutput, of the RF signal
- Comp Out, the output of the measurement comparator

Specifications:

- Vdd = 3V
- Idd = 50uA
- Pressure measurement range 0.8 to 1.3 Bars

- Calibration Capacitor: Poly Crystalline Silicone 85 um diameter
- Measurement Capacitor 10 pF that varies up and down and it not implemented on the chip
- Ring Oscillator Frequency 170-240MHz to avoid interference with 13.56 MHz.
- Band Gap Voltage = 1.2V

5.2 Schematics and simulation:

Bandgap reference:

Band Gap Circuit is shown in Figure.13 utilizes PTAT, CTAT references with self biased differential amplifiers. It shows zero temperature coefficient at 37°C. The temperature range chosen was from 30°C to 50°C shown in Figure 14, the variation over the range is 1mV. However, it had been noted that range of variations at various process corners is from 1.17 V to 1.24 V.

Specifications: The circuit must maintain a constant reference of 1.2 V at body temperature.

Real time Issues: There is more variation in Bandgap reference voltage with Vdd in the case of inductive power supply.

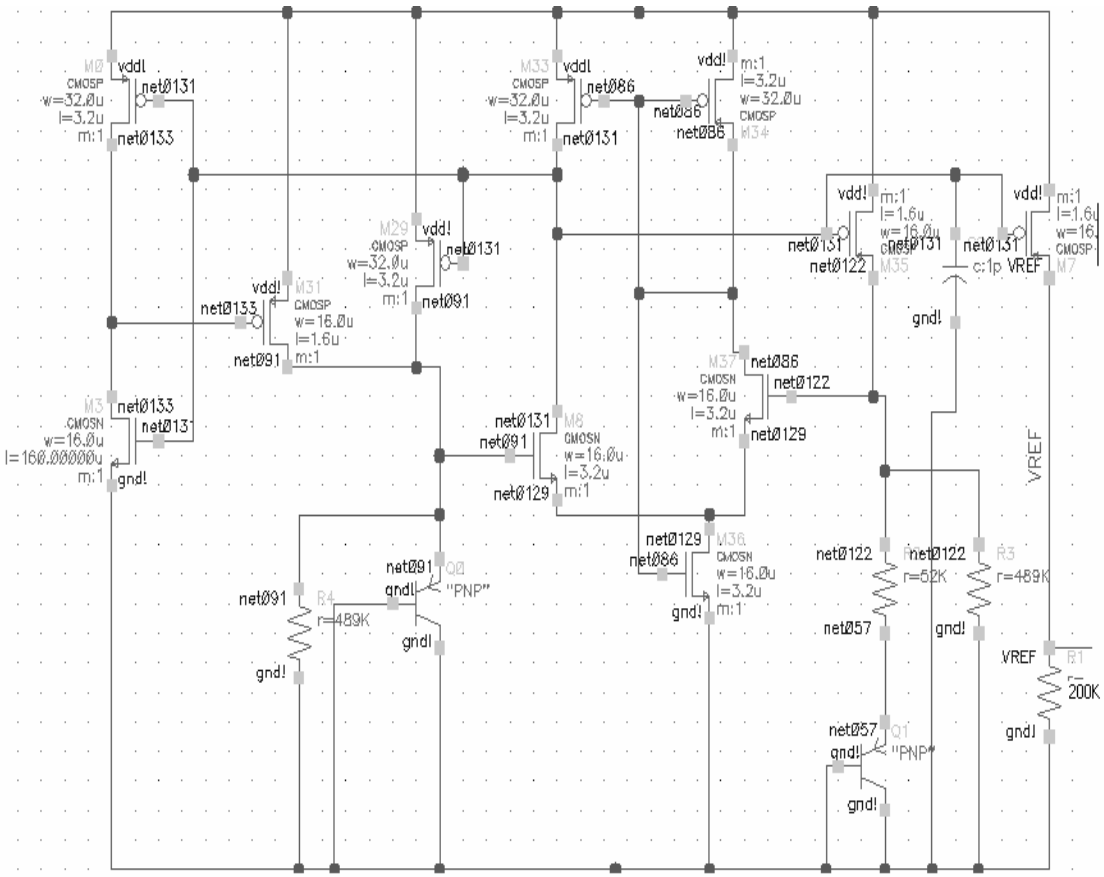

Figure 13. Bandgap reference generator.

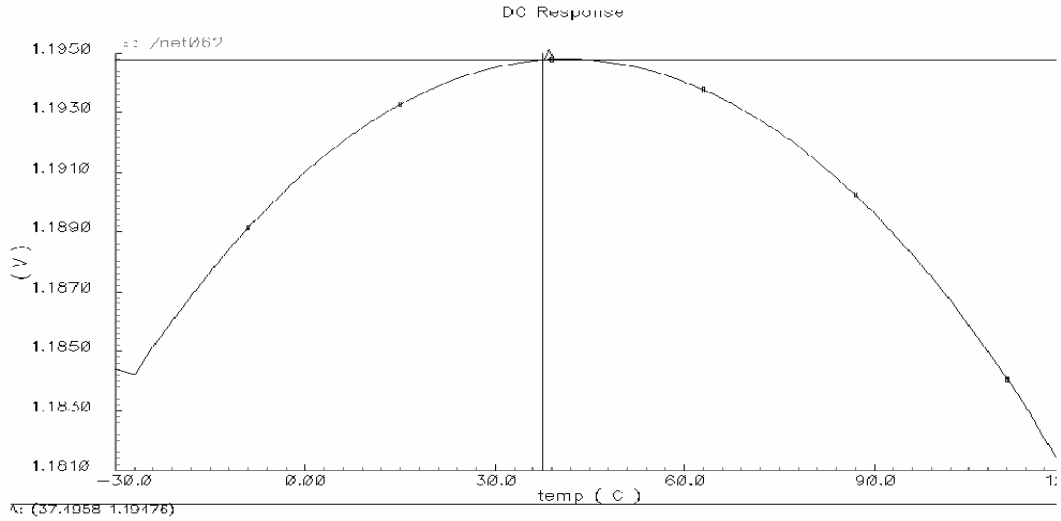

Figure 14. Band gap reference voltage generator temperature response.

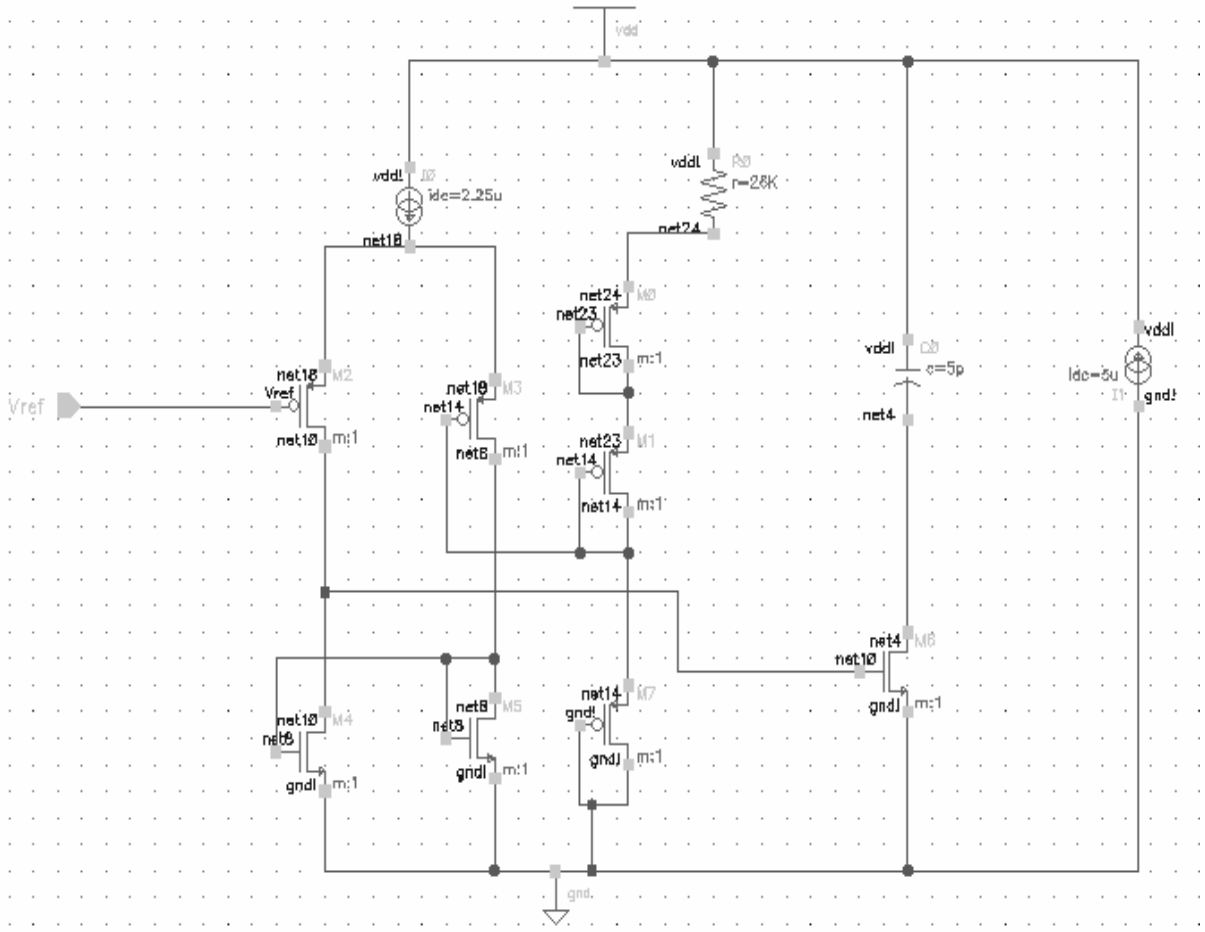

Figure 15. Implementation of shunt regulator. [23]

The strong dependence of the transmitted power through an inductive link on the link distance leads to large power fluctuations with small geometry shifts. This has traditionally been solved in implants by the use of zener diodes by simple p-n junction cascades as shunts across the supply. An active solution for this has several advantages over the passive diode based one. Low small signal resistance is desirable in the active region to set a predictable supply voltage independent of the shunt current.

Current Source:

Current reference produces a value of 4.7 uA. and the value was intended to be 5 uA but discrete channel length options caused the shift. However we are going to calibrate by placing the implant in a controlled pressure area and trim current or Vref to produce a know frequency to correspond to the controlled pressure in future.

Specifications: current = 5 uA.

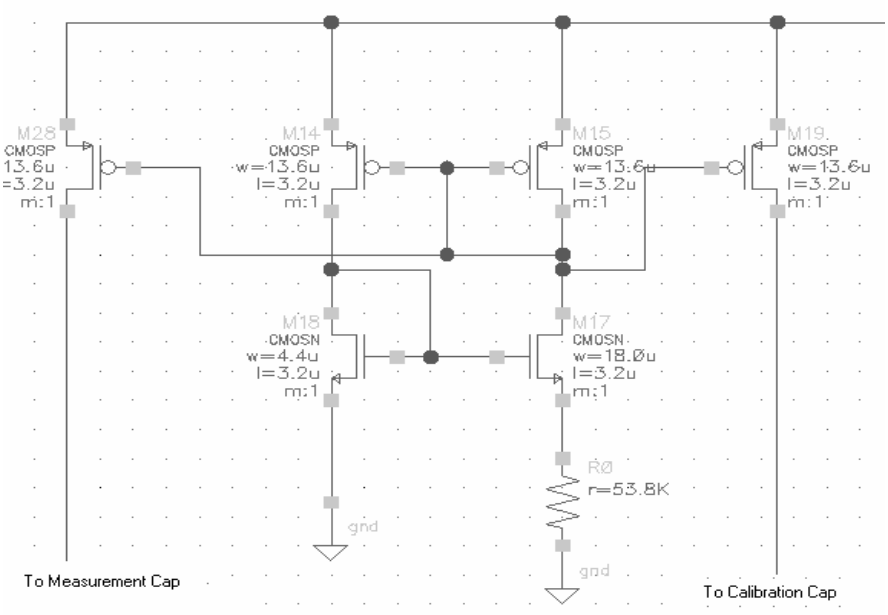

Figure 16. Current source.

Calibration and Measurement Capacitors and Comparator Circuit:

Comparator circuit consists of self biased differential pair and tail transistor. It compares the capacitor charge voltage to Band Gap reference and it produces a pulse that has a frequency value which correlates to the pressure on the measurement cap (Figure 18.).

Specifications: The circuit must produce a pulse with low On period and high Off period to reduce power consumption during transmission.

Issues: Calibration capacitor and initial charges in these capacitors have to be accounted.

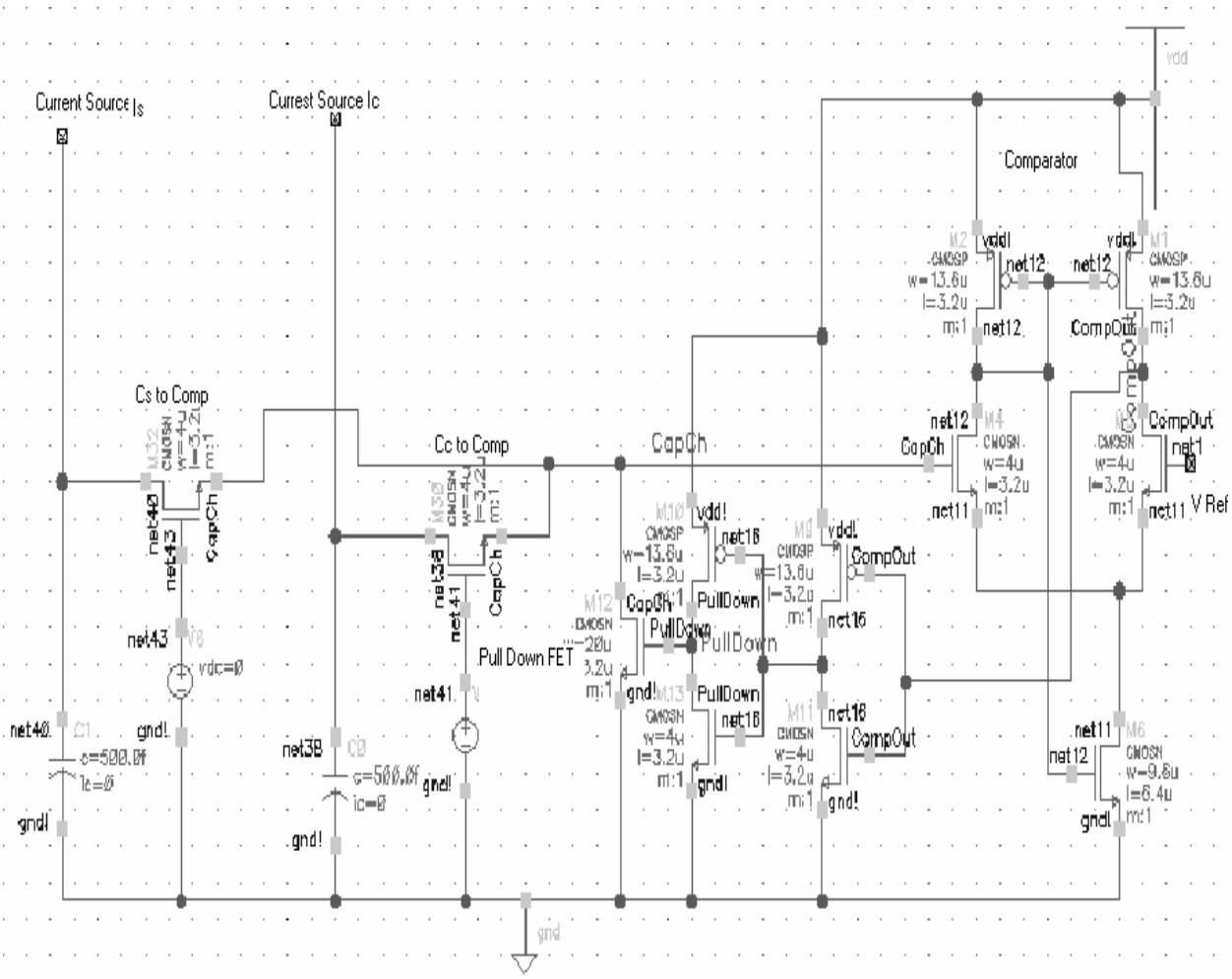

Figure 17. Calibration and Measurement Capacitors and Comparator Circuit.

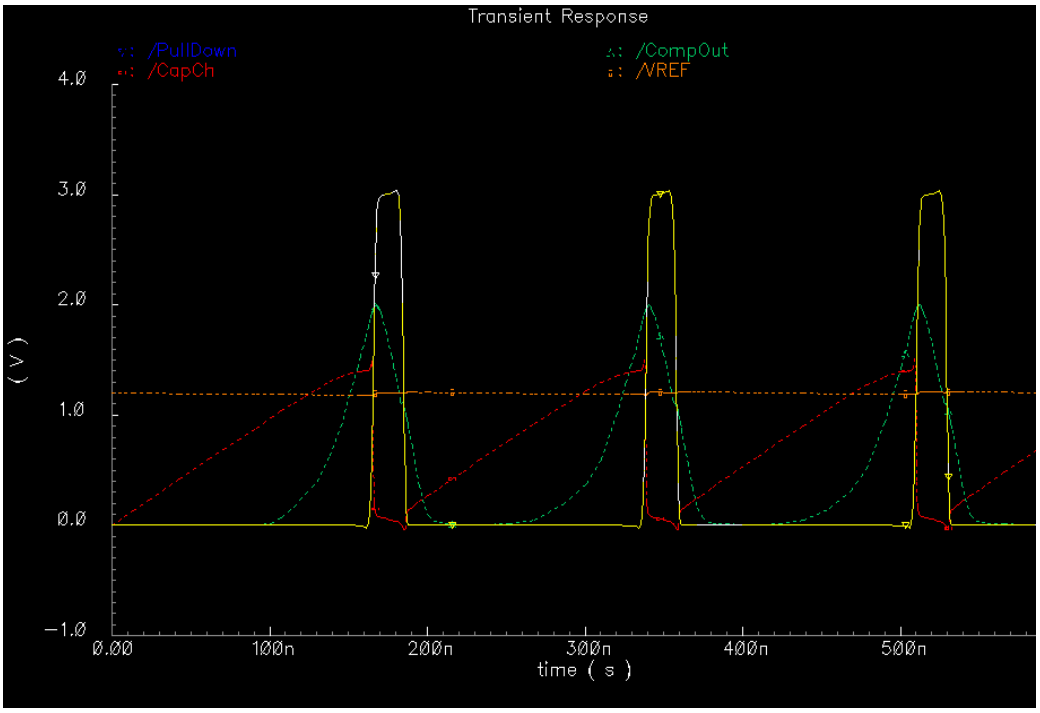

Figure 18. Output of Comparator Circuit.

Ring Oscillator:

Ring Oscillator: Consists of 3 inverters front to back as shown in Figure 19. The frequency it operates is 170-240MHz and the wide band specified is due to variation in process corners. The output pulse of the pressure reading is logically ANDed with the ring oscillator causing each pulse to be transmitted as stream of smaller pulses at RF signal levels.

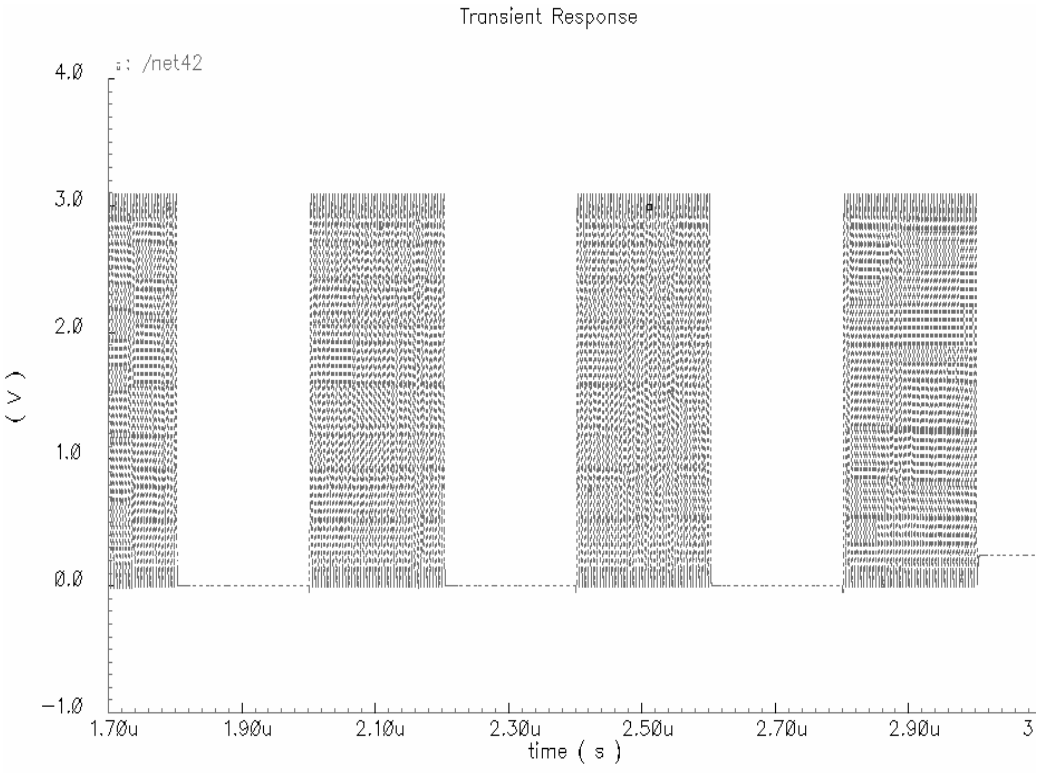

Figure 19. Ring oscillator output waveform.

Issues: Variation in the ring oscillator frequency is expected due to fabrication tolerances. The oscillator frequency also has dependence on Vdd partly due to dependence of Vref on Vdd. The variation in Band Gap Vref and Current source is due to the small head room. Such a problem will be overcome by trimming of charging current at Vdd=3V. When calibration starts at whatever Vdd value, the shift of frequency will be correlated to the shift in Vdd. The correlation factor will be also applied to the eye pressure value. The trimming will be done at 37^{o}C and 1 Atm and it will involve blowing poly fuses which add/subtract series connected resistanses in the current path. This will be implemented in the future.

Rectifier

The rectifier or power converter is the interface between the external RF signal and the internal power supply of the system. Since the quality of the power supply is influenced to a great degree by the signals passing through the rectifier it is necessary to examine in detail how system specifications affect the dimensions of the rectifying elements.

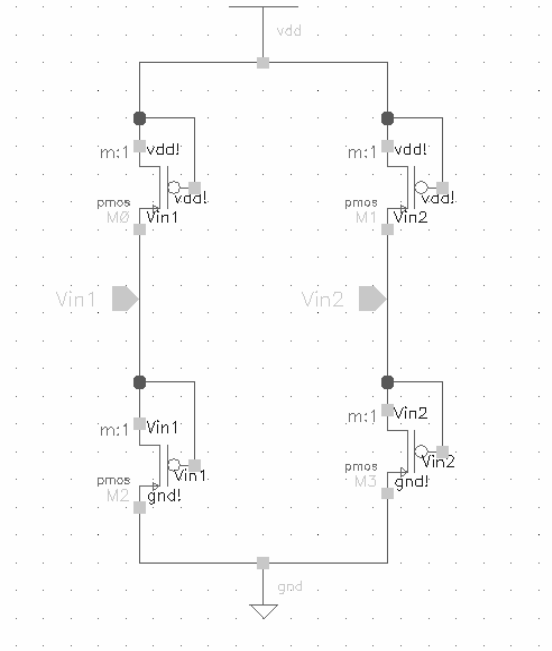

Figure 20. CMOS Full Bridge rectifier.

The power converter topologies found in literature are mostly full bridge rectifiers. The choice of the conversion circuit depends on the application; the main design challenge is to arrive at a compromise between power dissipation, area, input loading, and supply noise power spectrum. The above circuit has a full bridge rectifier implemented using diode connected pmos transistors.

Power on reset

As explained before, the power on phase of an implanted system must be controlled in such a way that the digital blocks if present must wake up in a known state. In the absence of an externally supplied reset signal the system must sense operating conditions correctly and generate an internal reset signal at the appropriate time. The specification of the reset operation depends on the nature of the processing elements within the system, but a wide range of combinations can be served by a relatively simple reset scheme. The pure analog elements should, if possible, be self starting.

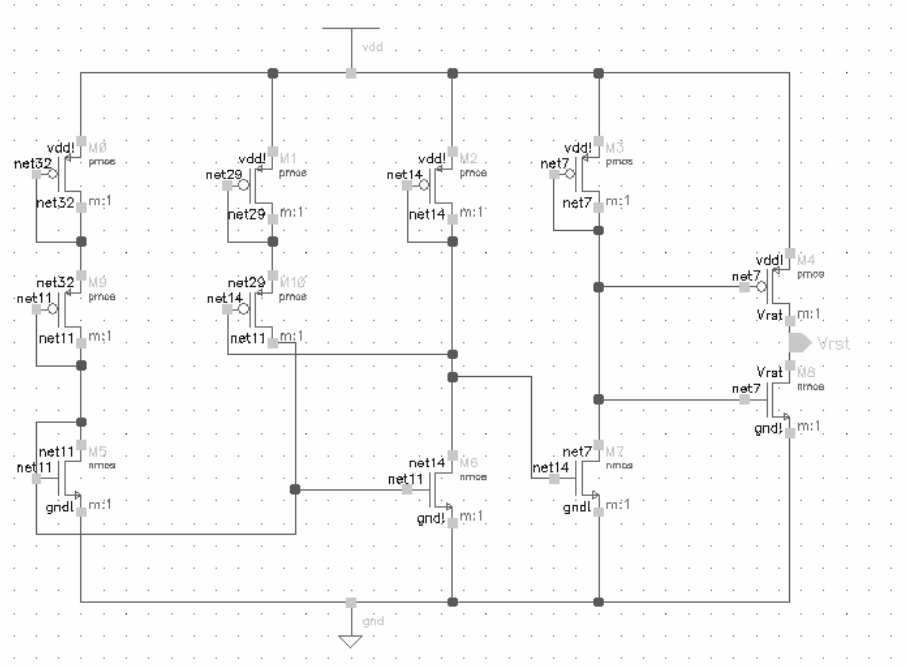

Figure 21. Power On reset circuit.

The supply current to the reset circuit is only 2uA which compares favorably with published power on reset circuits. The above circuit is an autonomous power on reset signal generator.

5.3 Layouts

The following section describes some of the layout tricks implemented in this design. The start up circuit circuit is implemented using a long channel transistor. In order to utilise the chip real estate efficiently and to reduce parasitics the following trick was followed. Figure 22a depicts the layout of a long channel transistor with its active area laid out in a serpentine pattern.

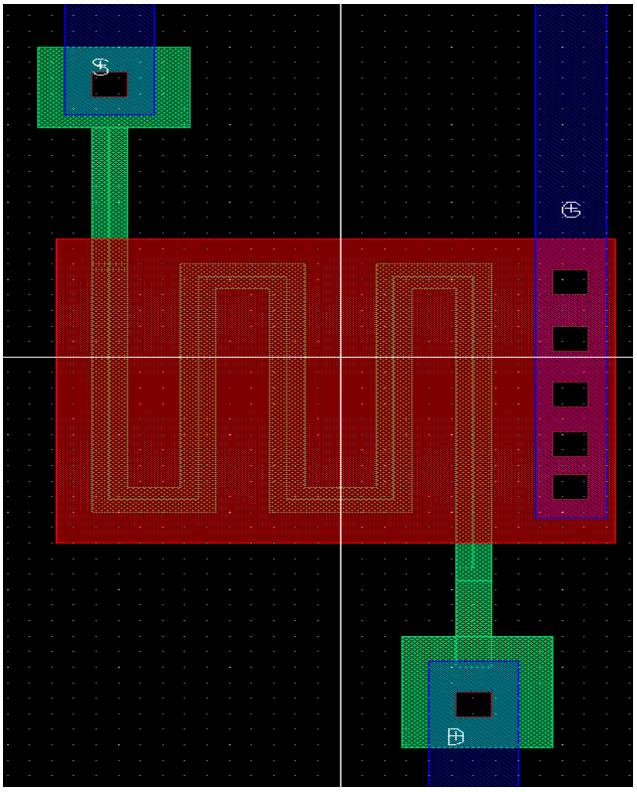

Figure 22a. A long gated device.

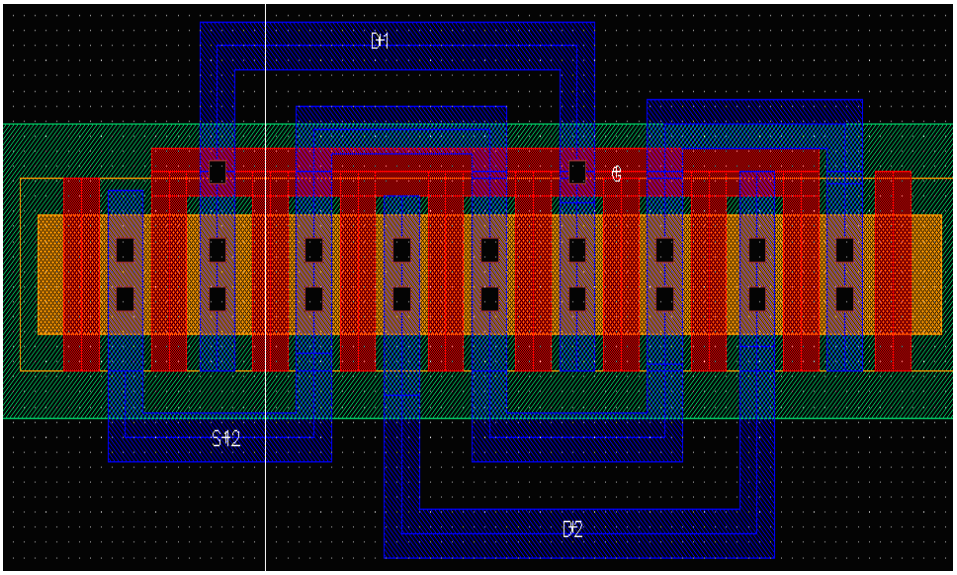

Figure 22b. Interdigitated current mirror.

For better matching between transistors forming current mirror, and to reduce parasitics, the above depicted interdigitated structure was implemented. Dummy polystrips reduce the variation between polystrips within the fingers of the transistors. Figure 22c shows the metal1 – metal2 calibration capacitor. As metal1-metal2 capacitors show less variation than the poly1-poly2 capacitors, the former was chosen in spite of their large area. Poly capacitance is very much process dependent and show much variation over the wafer due to the variation in thickness of their deposition, varying grain size whereas metal1- metal2 shows lesser variation.

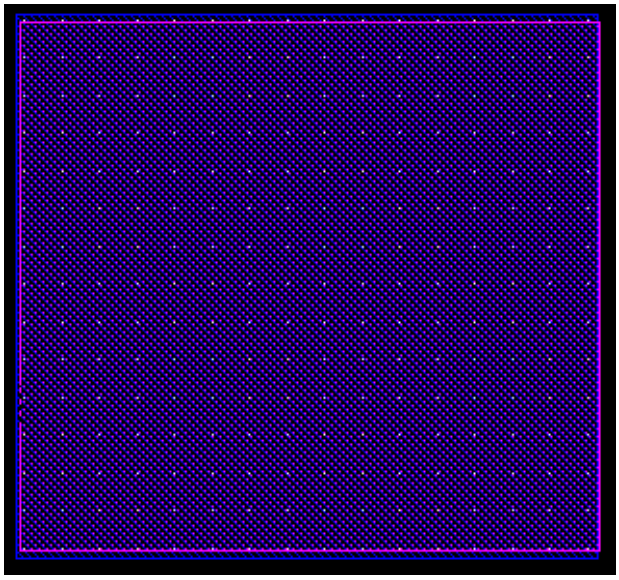

Figure 22c. Calibration capacitor.

Figure 22d shows the layout of the bandgap generator. It consists of four resistors, a metal2-metal1 capacitor, bipolar junction transistors with eight fingers. All MOS transistors have been laid out at the top using interdigitated layout. They have been made as compact as possible with sources of adjacent transistors in the circuit overlapped wherever possible.

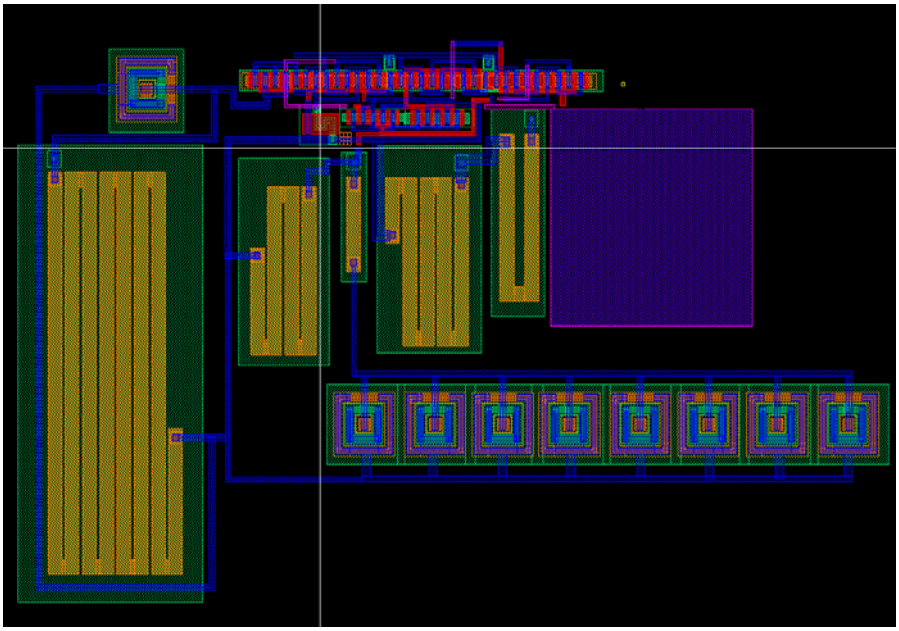

Figure 22d. Layout of Bandgap reference generator

Figure 22e shows the layout of comparator/measurement circuit. PBase resistors were used as they have the highest sheet resistance and smaller tolerance. It also conserves area.

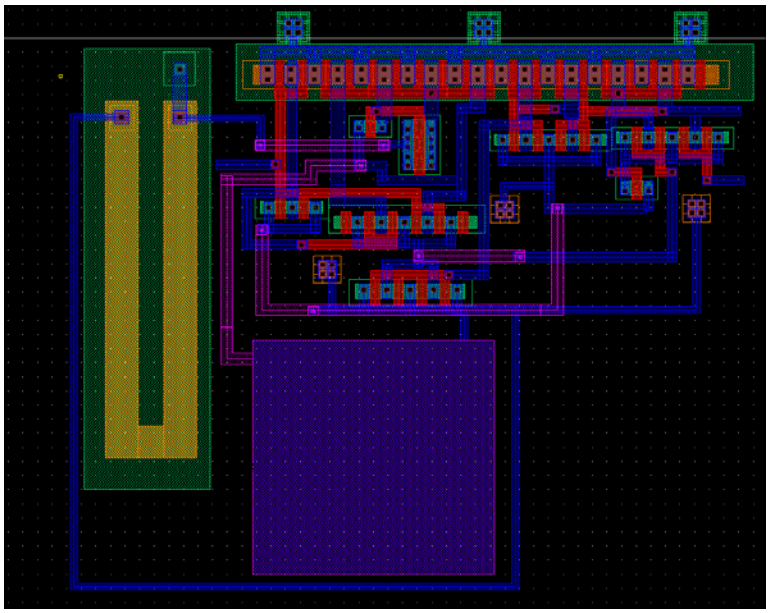

Figure 22e. Comparator and Measurement circuit.

Figure 22f shows the layout of ring oscillator. The circuit was intentionally not made compact as the parasitic capacitances are necessary to generate the required carrier frequency.

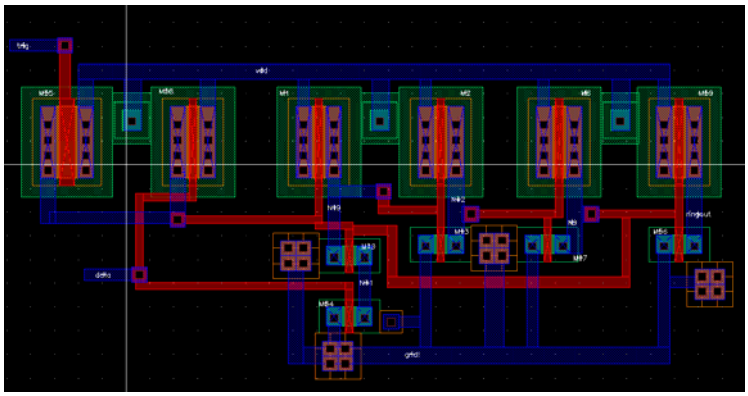

Figure 22f. Ring oscillator.

Figure 22g shows the complete layout of the circuit with p base resistors.

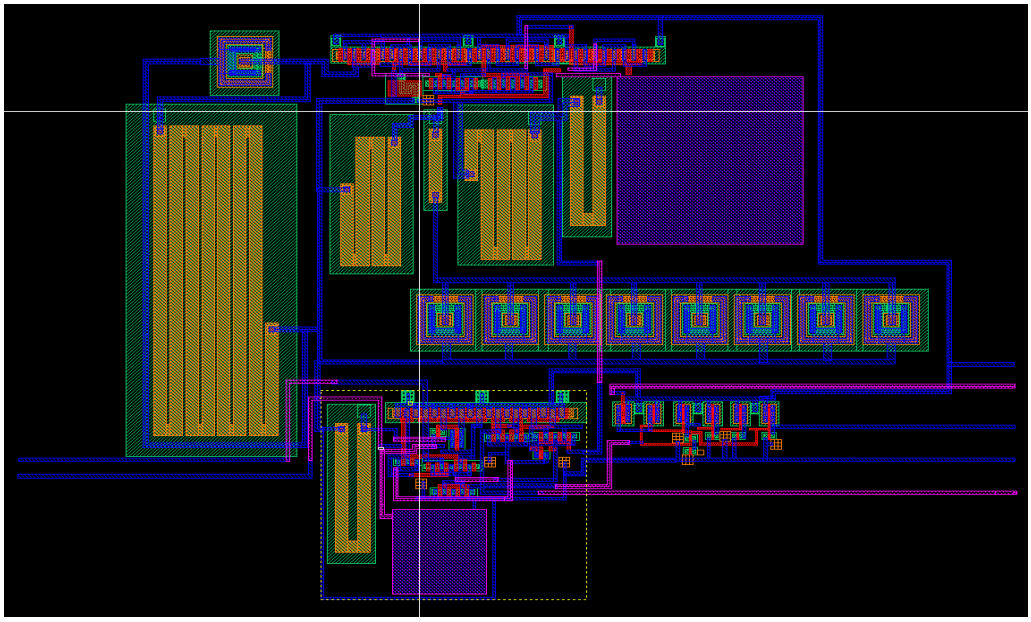

Figure 22g. Complete layout of the circuit.

In the above circuit p base resistors were considered to have a large tolerance in their values.

Hence all these resistors were replaced by poly resistors and is shown below.

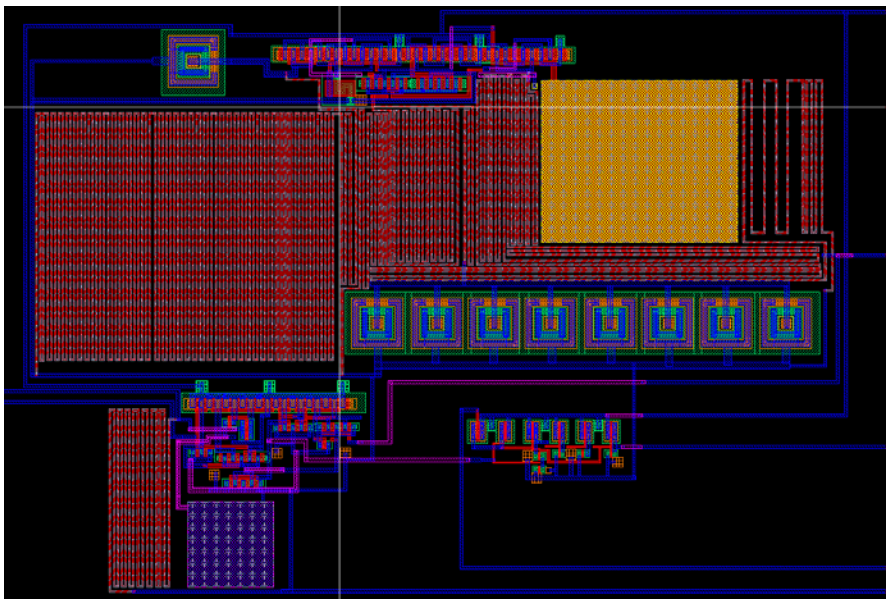

Figure 22h. Complete layout with poly capacitors and poly resitors.

5.4 Conclusion

The current design was compared with those of other peer groups. Table 1 shows the comparison of our results with peer groups. It indicates that our design is better than the existing Mokwa [2] design in power consumption which uses a similar principle.

Table 1. Comparison of our sensor with those of other groups.

Criterion for comparison	Mokwa et Al [17]	Wise [19]	Ziaie et al [20]	Collins [16]	Puers [18]	Our sensor
Pressure range	0.5-1.5 bar	>50 bar	>100 bar	Wider than 0.5-1.5 bar	0.5-1.5 bar	0.8-1.3 bar
Current consumption	<70 uA	<20uA	Not reported	Not reported	15 uA	50 uA
Power consumption	0.5 W	Not reported	Not reported	Not reported	Not reported	< 0.2 W
Frequency of operation	13.56 MHz	12 MHz	Around 34.6 MHz	Around 120 MHz	36-26 MHz	13.56 MHz/ 200 MHz
Operating temperature	0-80 ^{0}C	Not reported	Not reported	37C	Not reported	30 -130 ^{0}C
Data Transmission	Digital	Analog	Analog	analog	Analog	Analog
Power supply voltage	3 V	Not Known	Not Known	External supply 150 V	3V	3V

CHAPTER 6

DEVICE INTEGRATION

Device integration is a very important step as flaws in the integration leads to device failure. Packaging the integrated device is very important especially for a biomedical application in order to avoid infection. The analog circuit die after fabrication is solder bonded to another substrate wafer on which the sensor and macroscopic antenna are micromachined. This chapter deals with the integration of the sensor, antenna and the chip on a common substrate.

6.1 Materials for the pressure sensor:

The following materials have been studied for their suitability to the membrane electrode of pressure sensor. Research on some intelligent materials that suit our application has also been presented. Some of them are Monocrystalline silicon, Polycrystalline silicon, silicon nitride films, Polymers, and Elastomers.

Polysilicon:

Several groups have extensively studied the structural properties of polysilicon. For the membrane electrode of the capacitor, a highly doped polysilicon can be used. It has been reported that doped polysilicon structures deposited under normal IC conditions are in a state of compression that can cause mechanically constrained structures. It might make diaphragm like structures to buckle [24]. Another work suggests that by annealing at above 1000^0 C or by performing LPCVD at very low temperatures one can reduce significantly the residual strain in polysilicon employed for such thin membrane structure applications [25].

Polycrystalline silicon has also been studied and concluded as an effective material for capacitive sensor.

Silicon:

The availability of pure silicon crystals and ability to deposit high quality silicon films along with their excellent mechanical properties make them a choice to consider for our application. The stress concentrations in a thin membrane structure of silicon were studied by Mazza. The maximum force that could be applied on a thin silicon rod (40-60 micron) has been found to be 4.7N and the maximum average stress is 0.58 GPa. The elongation of thin silicon has also been studied and its failure most probably occurs at the contacts. The elasticity properties of micro silicon and bulk silicon coincide (they have almost same young's modulus). Several groups have studied the mechanical properties of thin silicon membranes obtained by bulk micromachining i.e forming the membrane by etching the substrate and also by surface micromachining the deposited thin layers of silicon.

Other materials:

Several other films made of silicon Nitride, chromium, Nickel have also been studied for their mechanical properties. The microfabrication technology used plays an important role in the strength of structures that are formed. For example, a column like grain structure is obtained for Nickel with the LIGA fabrication technique, which has strength values twice as the bulk nickel.

The first step while developing a new MEMS device is to decide upon the type of micro-machining technique to be used (bulk or surface). Reference [26] gives a detailed guide to select processes, depending on the materials used in the MEMS device. Surface micromachining involves deposition of thin films on the wafer surface followed by selective removal of one or more of these layers to leave freestanding structures such as membranes, cantilevers, bridges etc. It is different from bulk micromachining, which includes all techniques that remove significant amounts of the substrate. Surface micromachining allows complicated structures to be realized when compared to bulk micromachining. For the fabrication of the sensor, a combination of bulk and surface micromachining techniques are used. The bottom electrode is formed by bulk micromachining whereas the top structural member is surface micro-machined.

6.2 Etchants for sacrificial layer technology

Sacrificial etch:

Silicon oxide and silicon nitride (deposited) can act as sacrificial etches. Bassous and Bean have reviewed most popular etchants and attainable geometries for microelectromechanical structures. A detailed table of etchants for various material systems has been listed in [26]. Thus plenty of etchants are available in literature for any given material system (structure/sacrificial layer).

Certain measures have to be taken in order to overcome residual strain in the deposited structures. This involves choosing appropriate deposition conditions and careful optimization of the annealing step. A compatible set of sacrificial materials, structural materials and

chemical etchants have to be determined. The structural materials must have appropriate mechanical properties such as high yield and fracture strength, minimal creep and fatigue to prevent long time failure of the device.

Considering the above factors an analysis with respect to compatibility has been carried out and the results are described below.

Polycrystalline silicon and silicon dioxide:

It involves LPCVD deposition of Polysilicon and thermally grown or LPCVD deposition of SiO_2. The advantages of this combination are listed below.

- It is used in IC processing and their deposition technologies are readily available.
- Poly Si has excellent mechanical properties and can be heavily doped to form an electrode.

Polyimide and Aluminum:

Polyimide is used to make the structural element and aluminum is used as the sacrificial material. Acid based aluminum etchants are used to dissolve the sacrificial layer. The advantages of this combination are listed below.

- Polyimide has a small elastic modulus, which is 50 times smaller than the polycrystalline silicon.
- Polyimide can take large strains before fracture.
- Both polyimide and aluminium can be prepared at relatively low temperature.

The main disadvantage of polyimide is that it tends to drift and hence it exhibits some parametric drift which is absolutely not recommended for a safe biomedical application.

Silicon Nitride/Polycrystalline silicon:

Silicon Nitride is used as the structural element and polycrystalline silicon is used as the sacrificial layer. KOH and Ethylene Diamine Pyrocatechol are used to dissolve the Polysilicon.

Tungsten/Silicon dioxide:

Here tungsten is used as the structural element and Silicon dioxide as the sacrificial layer. HF is used as the etchant.

6.3 Process Flow for the pressure sensor

The following section makes use of the above study made on material systems and processes to design a fabrication flow for the sensor. The structural member chosen is polysilicon and the sacrificial layer chosen is silicon di oxide.

6.3.1. Front side Etch

1. On the substrate silicon wafer a thin oxide layer (about 200 nm) is grown.

2. The oxide layer is patterned to define regions for the forming the bottom electrode.

3. An orientation dependent etch such as KOH is used to define the front side etch. For making the front side etch, wet anisotropic etching can be carried out. Etchants such as KOH have etch rates close to 1.4 μm/min for the 100 plane and 0.003 μm/min for 111 plane for

materials with Zinc-Blende or diamond lattices. The other orientation dependent Etches are EDP (ethylene diamine pyrocarocatechol), Ammonium hydroxide etc. Precise V grooves in which edges are the (111) planes can be formed by this method.

6.3.2. Bottom Electrode for Capacitor

4. Pattern the oxide layer to define region for the N+ bottom electrode (1-1.2 mm).

5. A high conductivity N+ silicon layer is formed as the bottom electrode.

6.3.3. Membrane electrode for capacitor.

6. Surface micromachining procedures such as sacrificial layer technology can be employed for making the membrane electrode. Polycrystalline silicon is normally used for this process than monocrystalline silicon. A thin sacrificial layer of Silicon di oxide is deposited.

7. The SiO2 layer is patterned to deposit the support (anchor) for the membrane electrode and contacts to the Pd coil with the substrate.

8. A thin layer of polysilicon is deposited and then defined to form the top membrane electrode and small openings for the SiO2 etchant to reach sacrificial layers are defined.

9. Then polyimide supported coil is deposited and patterned.

10. Finally the structure is embedded in PDMS (silicone)

6.3.4. Fabrication Process Flow

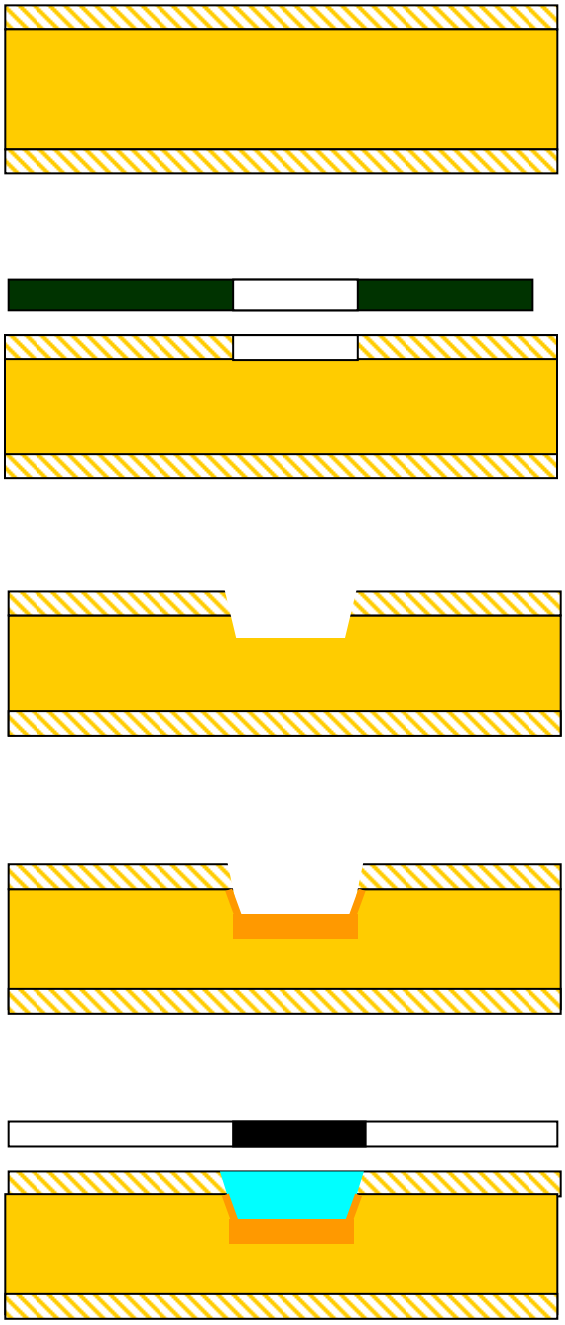

(1) Thermal oxidation of N-type wafer

(2) Patterning front side oxide to create cavity using **Mask 1**

(3) Formation of cavity for capacitor using orientation dependent etch (KOH)

(4) N+ diffusion to form bottom electrode of capacitor

(5) Deposition and patterning of Sacrificial etch (aluminum) **Mask 2 (mask1 can be reused using negative resist)**

Figure 23. Fabrication process flow of the sensor and antenna on a common substrate. (solder bonding to CMOS chip is not shown here)

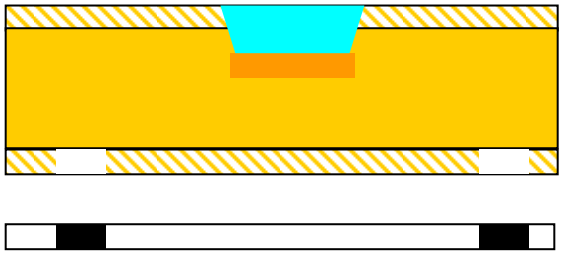

(6) Defining the backside etch regions in the thermal Oxide using **Mask 3**

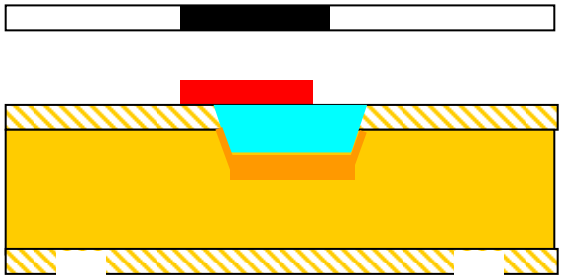

(7) Deposition of polysilicon and patterning it to form the top electrode of capacitor **Mask 4**

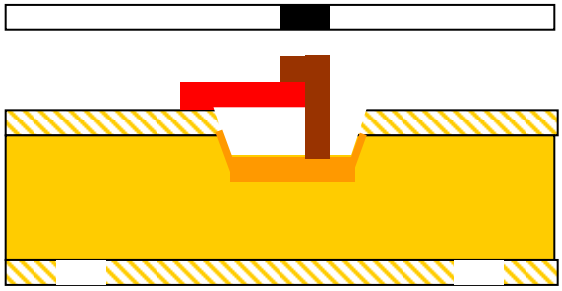

(8)Etching of sacrificial etch and formation of oxide seal using insulator using **Mask 5**

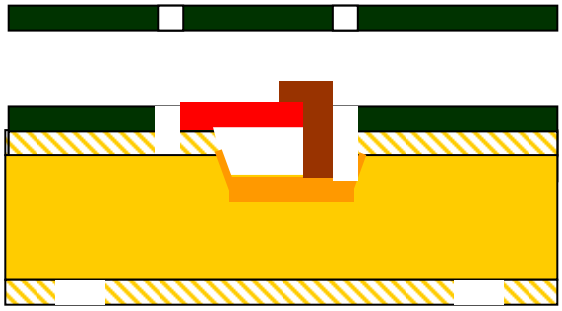

(9) Depositing polyimide and patterning it using **Mask 6** to form contacts with bottom electrode and substrate.

Figure 23. (..continued)

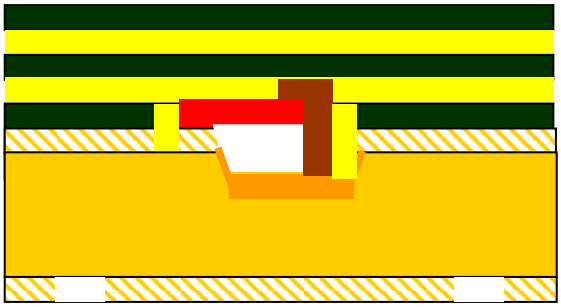

(10) Deposit layers of metal and polyimide and patterning them using **Mask 7**

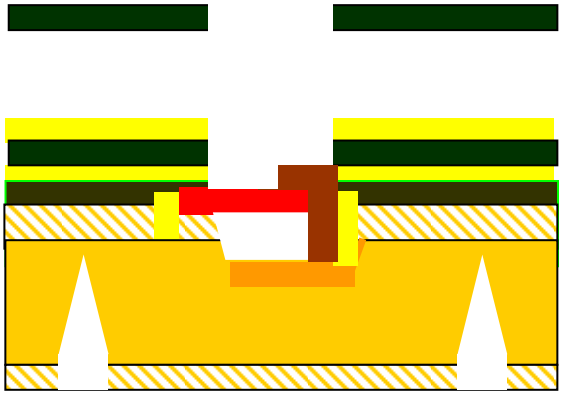

(11)Pattern layers of metal and polyimide using **Mask 4 (Shifted to the right),** followed by deposition of another metal level with an interlevel contact defined by **Mask 8,** followed by back door etching to release the sensor.

Figure 23 (..continued)

6.4 Integration of the Analog circuitry

The bare die with the necessary control and conditioning circuit is then attached to the solder balls. The solder balls sit on the pads leading to the interconnects on the common silicon substrate. The solder balls are then bonded in place with the pads. The interconnects carry the signals from the sensor to the circuit. These interconnects also interface with the actuator.

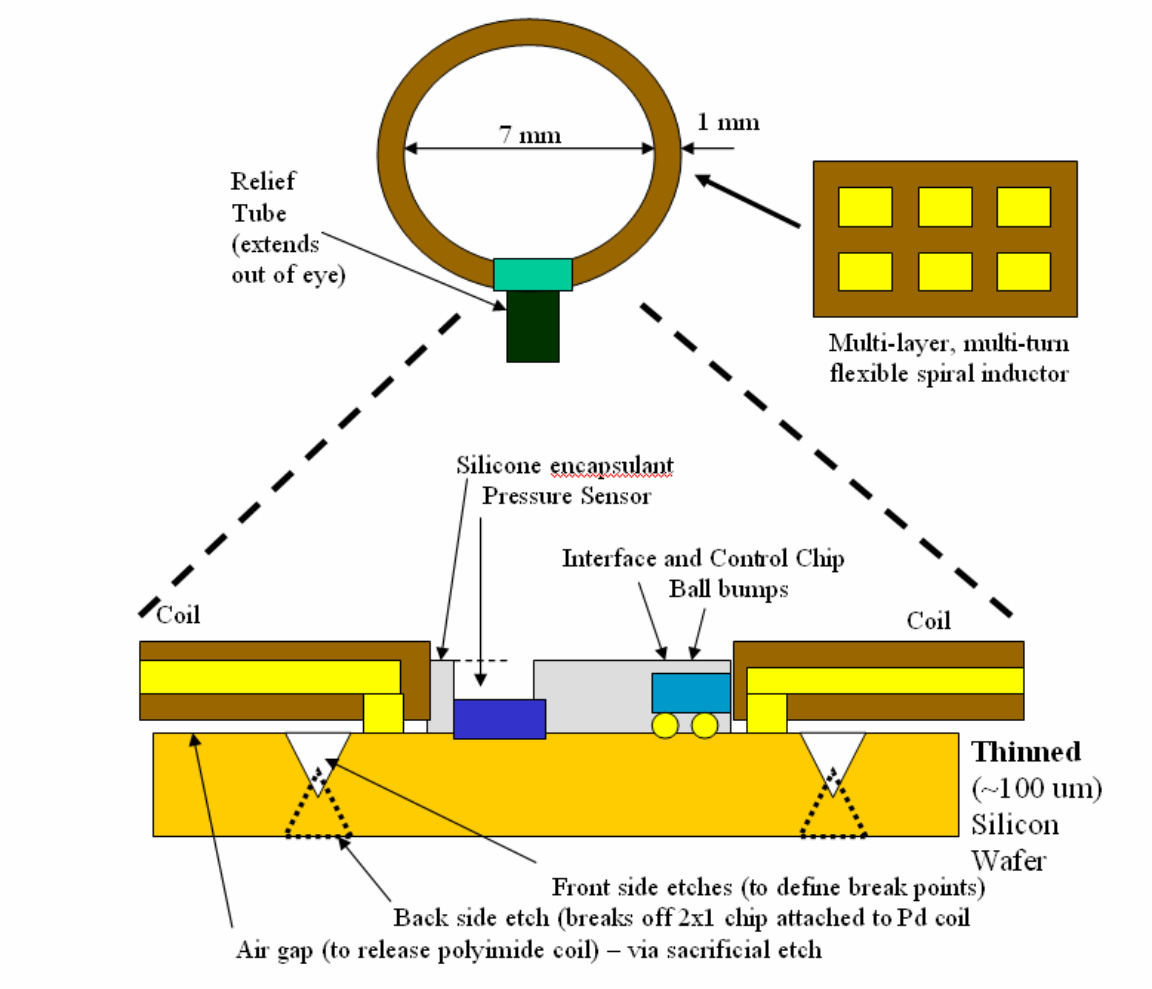

Figure 24. Overall Integrated system showing sensor and electronics solder ball bumped on a common substrate.

The above diagram does not show the interconnects which can be easily created by depositing and patterning metal layers. It can be seen that the top membrane of the capacitor is not covered with silicone.

6.5 Packaging

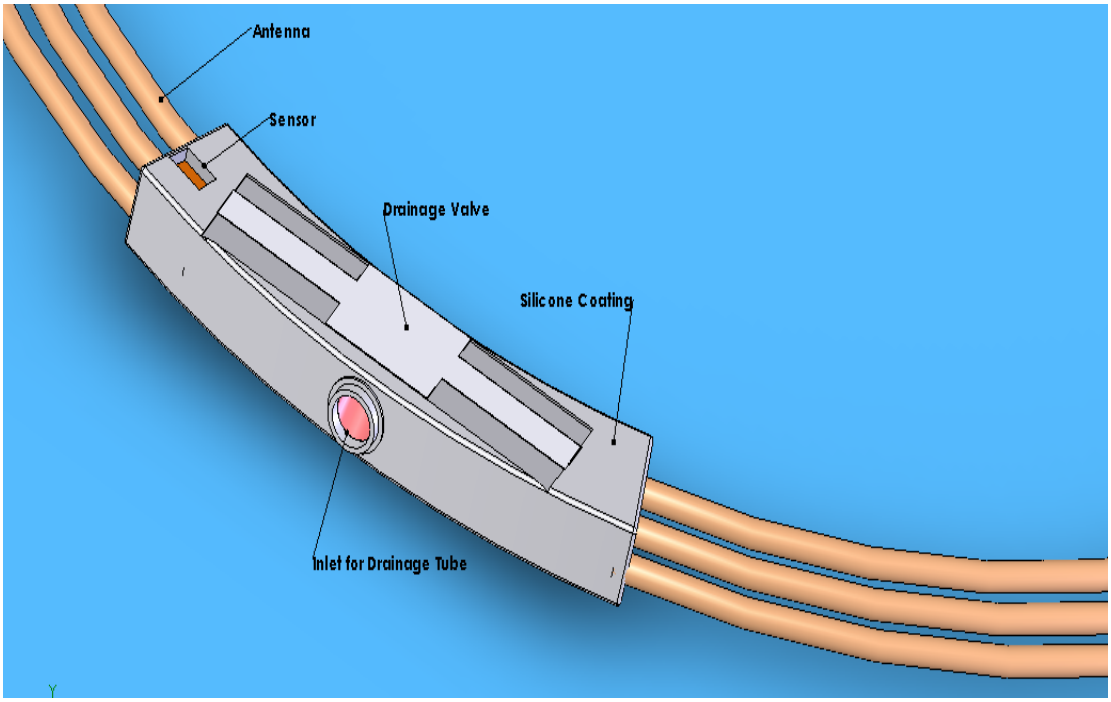

Figure 25. Complete device with silicone coating.

Packaging has been one of the most costly and least-developed aspects of Microsystems. It plays a special role in overall device performance. Suitable packaging of implantable biomedical devices pose a great challenge for the designers because not only do the devices need to remain functional, be protected from body fluids, and be able to communicate with their peripheries, but also the body needs to be protected from the materials used in microelectronics. The current project plans to use silicone coating as a barrier layer between the circuits and the body fluid. Silicone is the most compatible material to the body. Other suitable materials are pyrelene, silicone elastomers etc. All regions except the antenna are coated with silicone. The antenna is made of gold which is clinically proven as biocompatible.

CHAPTER 7

CONCLUSION

The design presented in this thesis report is only a portion of a complete system that can effectively control and manage glaucoma. However, this portion of the system compares well with those of other peer groups who have been working extensively in providing optimal solutions for continuous ocular pressure measurement as seen in chapter 5. The bottlenecks in the existing solutions have been effectively addressed in this design as physiology of the eye had been taken into account during the design stage. The success of this integrated device still lies largely on the biocompatibility of the system when implanted in a human body even though much attention has been paid to packaging of the system.

7.1 Issues to be Resolved

Some of the issues still to be investigated are

1. The reliability of interconnects on the common substrate and the losses involved have not been extensively studied yet.
2. The biocompatibility and electromagnetic field levels have to be thoroughly studied using a prototype before deploying it in a human eye.
3. The above two studies might necessitate deposition of additional layers such as electromagnetic shields around the device which might need some design modification.
4. The coupling of power in the implant antenna and the effect of rapid movements of eye on the coupled power need to be assessed experimentally.

7.2 Future work

Apart from resolving the above issues the future work will involve implementation of the remaining portion of the complete system i.e the actuator.

Glaucoma Drainage valve

The value addition to the system would be the glaucoma drainage valve that actuates based on the pressure sensed. This feature would revolutionize glaucoma management and control. The drainage tube can be co fabricated or a provision to insert the existing tube in the market must be made. The design of the drainage valve would involve analysis of various actuation mechanisms and then arrive at an optimal solution that is simple and also consumes minimal power. The success of this project would mean giving light to millions of eyes from a disorder that is the leading cause of blindness in the world.

REFERENCES

[1] Meindl JD., "Biomedical Implantable Microelectronics", *Science*, Oct 17, 1980; 210(4467):263-7.

[2] T. Akin and K. Najafi., "A telemetrically powered and controlled implantable neural recording system with CMOS interface circuitry" , *IEEE Proceedings of the Mediterranean Electro technical Conference (MELECON)*, Piscataway, New Jersey, USA,vol. 2, 1994, pp. 545-548.

[3] Quigley, H., "Number of people with Glaucoma worldwide", *British Journal of ophthalmology*, 1996. 80(5): pp. 389-393.

[4] Perkins, E.,"Hand-held applanation tonometer". *Br Journal of Opthalmology*, 1965. 49: pp. 591-593.

[5] Frenkel, R.,Y. Hong, and D.Shin, "Comparison of Tono-Pen to the Goldmann applanation tonometer". *Archives of Opthalmology*. 1998. 106(106): pp. 750-753.

[6] Zeimer, R., J. Wilensky, and D. Gieser, "Evaluation of a self tonometer for home use". *Arch Ophthalmol*, 1983. 101: pp. 1791-1793.

[7] Kothy, P., P. Vargha, and G. Hollo, "Ocuton-S self tonometry vs. Goldmann tonometry; a diurnal comparison study". *Acta Ophthalmol Scand*, 2001. 79: pp. 294-297.

[8] Pandav, S., A. Sharma, and A. Gupta, "Reliability of ProTon and Goldmann application tonometer in normal and postkeratoplasty eyes". *Ophthalmology.*, 2002. 109: pp. 979-984.

[9] Brandt JD, B.J., Kass MA,, "Central corneal thickness in the ocular hypertension treatment study (OHTS)". *Ophthalmology*, 2001. 108: pp. 1779-1788.

[10] Wilensky, J., Diurnal variations in intraocular pressure. *Tr Am Ophthalmol Soc*., 1991. LXXXIX:pp. 757-790.

[11] David, R., Z. L, and B. D, Diurnal intraocular pressure variations: an analysis of 690 diurnal curves. *Br J Ophthalmol*, 1992. 76: pp. 280-283.

[12] Zeimer, R., J. Wilensky, and D. Gieser, Association between intraocular pressure peaks and progression of visual field loss. *Ophthalmology*, 1991. 98: pp. 64-69.

[13] Asrani, S., et al., "Large diurnal fluctuations in intraocular pressure are an independent risk factor in patients with glaucoma". *Journal of glaucoma*, 2000. 9(2):pp. 34-42.

[14] Nouri-Madhavi K, Hoffman D, Coleman A, Gaasterland D,, Caprioli J. "Predictive Factors for Visual Field Progression in AGIS". *Ophthalmology,* 2004; 111:1627-1635.

[15] Data presented at the American Academy of Ophthalmology Annual meeting, 2003.

[16] Collins, C.C., "Miniature passive pressure transensor for implanting in eye", *IEEE Transactions on Bio-Medical Engineering,* BME-14, n 2, Apr, 1967: p 74-83.

[17] K. Stangel, S. Kolnsberg, Hammerschmidt, H. K. Trieu, W. Mokwa, "A programmable Intraocular CMOS pressure sensor system Implant", *IEEE Journal of Solid State* Vol. 36 No. 7 July 2001.

[18]J. Coosemans, M. Catrysse, R. Puers, "A readout circuit for an intra-ocular pressure sensor", Sensors and Actuators A 110 (2004) 432–438

[19] Andrew DeHennis and Kensall D. Wise, "A double-sided single-chip wireless pressure sensor", *The Fifteenth IEEE conference on Micro-Electromechanical systems.* Jan. 20-24, 2002,pp. 252-255, Las Vegas, NV, U.S.A.

[20] A. Baldi, W. Choi, B. Ziaie, "A self-resonant frequency-modulated micromachined passive pressure transensor**"** *IEEE Sensors Journal*, Vol. 3, Issue 6, Dec. 2003, pp.728 - 733

[21] Matteo Leonardi, Peter Leuenberger, Daniel Bertrand, Arnaud Bertsch, and Philippe Renaud. "First Steps toward Noninvasive Intraocular Pressure Monitoring with a Sensing Contact Lens". *Invest. Ophthalmol*. Vis. Sci. 2004 45: p3113-3117.

[22] www.fda.gov/cdrh/emc/wmt-about.html

[23] Gunnar Gudnason, Erik Bruun, "CMOS circuit design for RF sensors", Kluwer Academic Publishers, 2002.

[24] H Guckel et al, "Fabrication of micromechanical devices from polysilicon films with smooth surfaces", Sensors and actuators, Vol. 20, 1989, pp.117-122.

[25]Petersen et al, "Silicon as a mechanical material", Proceedings of IEEE, VOl. 70, 1982, pp.420-457.

[26] Patrick J. French, "Integration of MEMS devices", Electronics and structures for MEMS, Oct. 1999, Queensland, Australia.

[27] Ghovanloo.S, Atluri.S, "Design of a wideband Power-Efficient Inductive wireless Link for Implantable Biomedical devices using multiple carriers", Neural Engineering, 2005. Conference Proceedings, *2nd International IEEE EMBS Conference*, March 16-19, 2005 Page(s):533 - 537

[28] Leonardi,-Matteo, “First steps toward noninvasive intraocular pressure monitoring with a sensing contact lens”, Invest Ophthalmol Vis Sci -. 2004; 45(9): 3113-3117

[29] Rizq,-Raed-N, Choi WH, Eilers D, Wright MM, Ziaie B. “Intraocular pressure measurement at the choroid surface: A feasibility study with implications for implantable Microsystems”, British-Journal-of-Ophthalmology. 2001; 85(7): 868-871.

[30] Fleischman,-Aaron-J, “Intraocular pressure measurement system including a sensor mounted in a contact lens”, Official-Gazette-of-the-United-States-Patent-and-Trademark-Office-Patents. 2004; 1283(3)

[31] Tamaki,-Yasuhiro, “Non-contact, two-dimensional measurement of tissue circulation in choroid and optic nerve head using laser speckle phenomenon”, Experimental-Eye-Research. 1995; 60(4): p373-383.

[32] Harada Y, Naoi N. “Corneal elasticity as a measure of intra-ocular pressure: a controlled clinical examination.” Kobe J Med Sci. 2004;50(5-6): p141-52.

[33] Hallberg P, Linden C, Lindahl OA, Backlund T, Eklund A. “ Applanation resonance tonometry for intraocular pressure in humans.”, Physiol Meas. 2004 Aug;25(4):1053-65.
Guttmann C, “Mini shunt diverts excess aqueous humor”, Ophthalmology Times, Nov 15, 2004, pp 34.

APPENDICES

APPENDIX A

MATLAB SCRIPT FOR LINK DESIGN

The script given below can be used to generate a antenna system comprising of a primary and secondary coil for any dimensions specified by the user. The script runs in any version of MATLAB. It can be useful for antenna design for any application.The generated file can be used with Electromagnetic field solving tools.

```
%********* File to Generate primary and secondary coils for an inductive link*******************

disp('Please enter the radius of the secondary coil in mm');
r = input('');
theta = input(' Enter the angle defining resolution      ');
rad = (theta/180)*3.142;
N = 360/theta;
int w;
int h;
int sw;
int sh;
int ntr;
int nt;
int nlr;
int nl;
 w = input ( ' Enter the width of the secondary  coil in mm      ');
 sw =input (' Enter the separation between turns of the coil in a layer in mm   ');
 h = input (  ' Enter the height of the secondary coil   in mm    ');
 sh = input (  ' Enter the separation between  layers of the coil  in mm      ');
 nt = (0.5 - (sw))/(sw + w);
 ntr = int8(nt) ;
    if (ntr > nt)
    ntr = ntr-1;
    end
 nl = (0.3 - (sh))/(sh + h);
 nlr = int8(nl) ;
```

```
    if (nlr > nl)
    nlr = nlr-1;
    end

 disp(' Due to restricted space available in the eye      ');
 disp( ' The total number of turns that can be accomodated in a single layer is   ');
 disp (ntr);
 disp( ' The total number of layers that can be accomodated  is   ');
 disp (nlr);

%  generating the coordinates of the secondary coil
xp=0;
yp=0;
i = 0;
k=0;
xs = zeros(N,1);
ys = zeros(N,1);

for i= 1:1:N
    xs(i) = r*cos(k);
    ys(i) = r*sin(k);
    k = k+ rad;
end
t=N;

while ntr>1

   r = r+sw;
   k = 0;
   for i = (t+1):1:(t+N)
       xs(i) = r*cos(k);
       ys(i) = r*sin(k);
       k = k+ rad;
   end
   ntr = ntr -1;
   t = t+N ;
end

  fid = fopen('c:/coil.inp', 'wt' );
  fprintf(fid,'**********Generating the primary and secondary coils made of
copper*****************\n')
  fprintf (fid,'.units mm\n');
  fprintf( fid,'.default z=0 sigma=5.8e4\n');
  for i = 1:1:t
```

```
  fprintf(fid , 'N%d x = %6.2f y = % 6.2f\n',i, xs(i) , ys(i));
 end
 stat =t;
 size=t;
 en = 1;
 r =t;
 c= -1;
 while nlr>1
      for i = stat:c:en
      r = r+1;
      fprintf(fid , 'N%d x = %6.2f y = % 6.2f   z = %6.2f\n',r, xs(i) , ys(i), (sh+h));
      end
      nlr = nlr - 1;
      sh=sh+h+h;
      if rem(nlr,2) == 0
         stat = 1;
          en = size;
          c=1;
      end
       if rem(nlr,2) == 1
            stat =size;
             en= 1;
             c=-1;
          end
 end

 for i = 1:1:(r-1)
    j =i+1;
    fprintf(fid,'E%g N%g N%g w=%6.2f h=%6.2f \n' , i,i, j, w, h);
 end


disp('Please enter the distance in mm between the primary and the secondary coil');
dist = input ('');
disp('Please enter the radius of the primary coil');
r = input('');

w = input ( ' Enter the width  ');
hp = input (  ' Enter the height   ');
swp = input (  ' Enter the distance between the turns          ');
nlrp = input (  ' Enter the number of layers  ');
shp = input (  ' Enter the distance between the layers          ');
rout =1.2*r;
ntrp = (rout -r- (swp))/(swp + w);
```

```
xp = zeros(N,1);
yp = zeros(N,1);
k=0;

for i= 1:1:N
    xp(i) = r*cos(k);
    yp(i) = r*sin(k);
    k = k+ rad;
end
%%%%%%%%%%%%%%%%%%%
t=N;

while ntrp>1

   r = r+swp;
   k = 0;
   for i = (t+1):1:(t+N)
       xp(i) = r*cos(k);
       yp(i) = r*sin(k);
       k = k+ rad;
   end
   ntrp = ntrp -1;
   t = t+N ;
end

  for i = 1:1:t
    fprintf(fid , 'Np%d x = %6.2f y = % 6.2f z = % 6.2f\n',i, xp(i) , yp(i),dist );
  end
  stat =t;
  size=t;
  en = 1;
  r =t;
  c= -1;
  while nlrp>1
        for i = stat:c:en
        r = r+1;
        fprintf(fid  ,  'Np%d  x  =  %6.2f  y  =  %  6.2f      z  =  %6.2f\n',r,  xp(i)  ,  yp(i),
(dist+shp+hp));
        end
        nlrp = nlrp - 1;
        shp=shp+hp+hp;
        if rem(nlrp,2) == 0
           stat = 1;
            en = size;
            c=1;
```

```
        end
         if rem(nlrp,2) == 1
              stat =size;
               en= 1;
               c=-1;
            end
  end

  for i = 1:1:(r-1)
      j =i+1;
      fprintf(fid,'Ep%g Np%g Np%g w=%6.2f h=%6.2f \n' , i,i, j, w, h);
  end
%%%%%%%%%%%%%%%%%%
fmin = input(' Enter the minimum frequency       ');
fmax = input(' Enter the maximum frequency       ');
ndec = input('Enter the number of frequencies to be analysed in a decade      ');
fprintf(fid,'.freq fmin=%d fmax=%d ndec=%d\n',fmin,fmax,ndec);
 fprintf(fid,'.end');
```

APPENDIX B

Terminology related to the structure of Human Eye

Optic nerve: The bundled collection of the retinal nerve fiber layer which transmits visual information from the eye to the brain.

IOP Normal range: The normal eye pressure range is 10-21 mm Hg above atmospheric pressure 1atm = 760 mm Hg = 760 torr.

Trabecular Meshwork: A network of fibers that is responsible for draining aqueous humor from the eye.

Ciliary body: The thickened vascular portion of the eye that lies between iris and the choroids. It is responsible for the formation of aqueous humor in the eye.

Canal of Schlemm: A circular canal between the iris and cornea. This canal provides an exit for the aqueous humor from the eye to the blood stream.

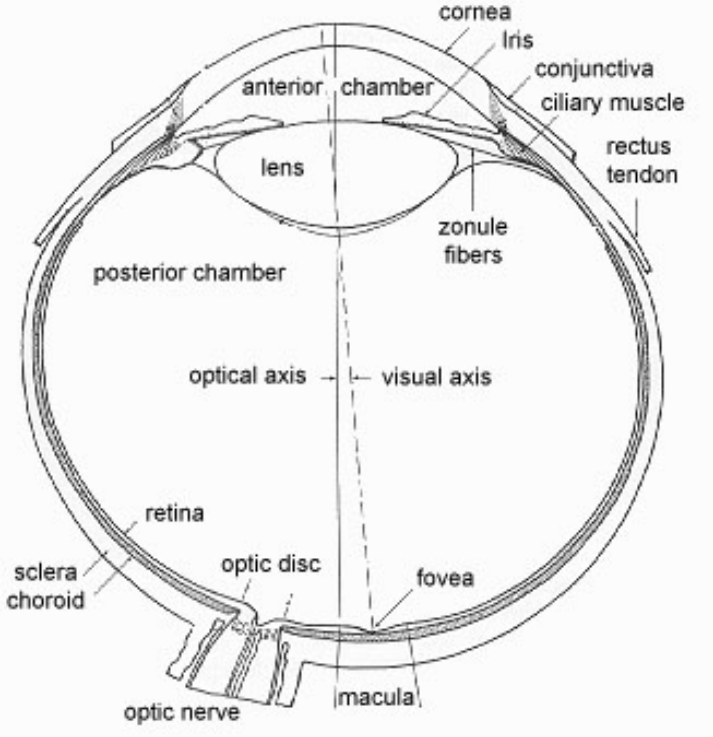

Figure 26. Structure of a Human Eye.

Ref: people.eku.edu/ ritchisong/eye.JPG